



HAL
open science

A Mixed-Signal Oscillatory Neural Network for Scalable Analog Computations in Phase Domain

Corentin Delacour, Stefania Carapezzi, Gabriele Boschetto, Madeleine Abernot, Thierry Gil, Aida Todri-Sanial

► **To cite this version:**

Corentin Delacour, Stefania Carapezzi, Gabriele Boschetto, Madeleine Abernot, Thierry Gil, et al.. A Mixed-Signal Oscillatory Neural Network for Scalable Analog Computations in Phase Domain. 2023. hal-03961010

HAL Id: hal-03961010

<https://hal.science/hal-03961010>

Preprint submitted on 31 Jan 2023

HAL is a multi-disciplinary open access archive for the deposit and dissemination of scientific research documents, whether they are published or not. The documents may come from teaching and research institutions in France or abroad, or from public or private research centers.

L'archive ouverte pluridisciplinaire **HAL**, est destinée au dépôt et à la diffusion de documents scientifiques de niveau recherche, publiés ou non, émanant des établissements d'enseignement et de recherche français ou étrangers, des laboratoires publics ou privés.

Copyright

A MIXED-SIGNAL OSCILLATORY NEURAL NETWORK FOR SCALABLE ANALOG COMPUTATIONS IN PHASE DOMAIN

A PREPRINT

Corentin Delacour¹ Stefania Carapezzi¹ Gabriele Boschetto¹ Madeleine Abernot¹ Thierry Gil¹

Aida Todri-Sanial^{1,2}

¹ Microelectronics Dept., LIRMM, University of Montpellier, CNRS, France

² Electrical Engineering Dept., Eindhoven Technical University, Netherlands

{firstname.lastname}@lirmm.fr

ABSTRACT

Digital electronics based on von Neumann’s architecture are reaching their limits to solve large-scale problems essentially due to the memory fetching. Instead, recent efforts to bring the memory near the computation have enabled highly parallel computations at low energy cost. Oscillatory Neural Network (ONN) is one example of in-memory analog computing paradigm consisting of coupled oscillating neurons. When implemented in hardware, ONNs *naturally* perform gradient descent of an energy landscape that makes them particularly suited for solving optimization problems. Although the ONN computational capability and its link with the Ising model are known for decades, implementing a large-scale ONN remains difficult. Beyond the oscillators’ variations, there are still design challenges such as having compact, programmable synapses and a modular architecture for solving large problem instances.

In this paper, we propose a mixed-signal architecture named *Saturated Kuramoto ONN* (SKONN) that leverages both analog and digital domains for efficient ONN hardware implementation. SKONN computes in the analog phase domain while propagating the information digitally to facilitate scaling up the ONN size. SKONN’s separation between computation and propagation enhances the robustness and enables a feed-forward phase propagation that is showcased for the first time. Moreover, the SKONN architecture leads to unique binarizing dynamics that are particularly suitable for solving NP-hard combinatorial optimization problems such as finding the Weighted Max-cut of a graph. We find that SKONN’s accuracy is as good as the Goemans-Williamson 0.878-approximation algorithm for Max-cut; whereas SKONN’s computation time only grows logarithmically. We report on Weighted Max-cut experiments using a 9-neuron SKONN proof-of-concept on PCB. Finally, we present a low-power 16-neuron SKONN integrated circuit and illustrate SKONN’s feed-forward ability while computing the XOR function.

Keywords Oscillatory Neural Network, Analog Computing, Mixed-signal design, NP-hard problems

1 Introduction

1.1 Oscillatory Neural Networks

The synchronization of oscillators is a fascinating phenomenon studied for a long time. In the XVII century, Huygens noticed that two identical clocks attached to the same beam synchronize to an anti-phase state where the two pendulums have the same frequency and move in opposite directions [1]. It is in the 1950s that scientists imagined computing with coupled oscillators. The main motivation at that time was to replace the bulky and slow vacuum tubes used for

Table 1: State-of-the-art ONN architectures

	Goto [3]	Jackson et. al. [5]	Wang et. al [17].	Chou et. al [18].	Bashar et. al [19].	Dutta et. al [9].	Ahmed et. al [11].	Graber et. al [20].	This work
Size	9600	100	240	4	30	8	560	400	16
Oscillator	Analog LC	Digital	Analog LC	Analog LC	Analog relaxation	Analog relaxation (PTNO)	Ring Oscillator	Analog differential	Analog relaxation
SHIL or Calibration	Yes	Yes	Yes	Yes	Yes	Yes	No	Yes	Yes
Coupling	Transformers	Resistors	Resistors	Resistors	Capacitors	Capacitors Resistors	B2B inverters	Current sources with DACs	Capacitors
Signed weights	No	Yes	Yes	Yes	No	No	Yes	Yes	Yes
Weight precision	1 bit	5 bits	8 bits	5 bits	1 bit	-	-1,0,+1	6 bits	5 bits
Modular	Yes	-	Yes	-	-	-	Yes	Yes	Yes
Feedforward	Yes	Yes	-	Yes	No	No	No	Yes	Yes
Initial phase control	Yes	Yes	-	-	-	-	-	No	Yes
Application	Digital logic	Pattern recognition	COP	COP	COP	COP	COP	COP	COP Image processing

digital computations. In 1954, von Neumann proposed in a patent to use LC resonant circuits driven by a harmonic signal to compute digital functions [2]. At the same time in Japan, Goto developed a similar paradigm called the *parametron*, which consists of an LC resonant circuit oscillating at one-half the driving frequency. Using transformers as coupling elements, Goto was able to build multiple large-scale digital computers with up to 9600 parametrons in 1958 [3]. However, parametrons became obsolete in the 1960s due to the advent of transistors that were faster and more scalable. [4].

With the emergence of Artificial Intelligence (AI) and neural networks, researchers brought back the idea of phase computing to solve complex tasks like pattern recognition [5, 6, 7] and NP-hard combinatorial optimization problems (COPs) [8, 9, 10, 11] that are challenging for conventional digital electronics. Inspired by Hopfield Neural Networks (HNN) [12] and by the Kuramoto model [13], Aoyagi [14], Hoppensteadt and Izhikevich [15] have proposed a computing paradigm called *Oscillatory Neural Networks* (ONN) that models the phase dynamics of coupled oscillators. ONNs are particularly interesting for solving COPs as they are dynamical systems that converge *naturally* to fixed points corresponding to the minima of some energy landscape. In other words, there is no external control that makes the neuron state evolve. Instead, all the phases evolve in parallel and in continuous time, enabling fast and energy-efficient inferences in the analog domain [16].

1.2 State-of-the-art ONNs

Recently, a new interest in ONN has risen thanks to the emergence of novel oscillating devices that enable the fabrication of efficient ONNs [21]. Such as, spin-torque and spin Hall devices [22, 23], micro-electromechanical systems [24, 25], and transition metal oxide devices are all candidates for implementing ONNs using their oscillatory behavior and synchronization properties [6, 9, 26, 27, 28]. Beyond-CMOS devices are promising as they generally allow a compact oscillator design using a single device that could be scaled down to the nanoscale. Nevertheless, CMOS-based ONNs benefit from the mature CMOS technology which enables rapid ONN development and facilitates its co-integration with conventional digital circuits [5, 11, 19, 20]. In this work, we focus on ONNs that compute in phase domain, i.e. with neurons that oscillate at the same frequency. However, note that it is also possible to compute with various frequencies [29, 30]. Regardless of the technology, we identify three important criteria for designing a competitive ONN that computes in phase domain. It should have:

1. Homogeneous oscillating frequencies
2. Compact and linearly programmable signed synapses
3. A scalable architecture

Even with the mature CMOS technology, achieving perfect matching between hundreds of oscillators is unfeasible for small-scale oscillators due to device-to-device variations. Hopefully, some techniques can overcome frequency mismatches such as calibration or Sub Harmonic Injection Locking (SHIL). SHIL consists in driving the oscillators with a harmonic signal that can lock to a Fourier harmonic of the oscillating signal [31]. In case of large frequency mismatches, the injection of a strong SHIL signal ensures phase locking among the oscillators [32, 33]. The second

criterion promotes synapses that are compact, programmable with signed weights, and have a value proportional to their conceptual weight. Some architectures can lead to a non-linear mapping between the conceptual weights and their hardware implementation [34], or even be unknown due to the high complexity of the dynamics. Finally, the ONN architecture must be scalable to compete with conventional computing and solve large-scale problems involving thousands or millions of synapses. For this reason, we believe that the ONN architecture should be modular, i.e. to support the interconnection of smaller sub-ONNs to build a larger system and avoid the implementation of a fully-connected network.

Table 1 presents the state-of-the-art ONN architectures and their features. We only consider ONN computing in the phase domain and based on electrical oscillators. For solving COPs, a general approach is to map the input graph to the ONN where vertices are oscillators, and edges are synapses. Some architectures such as [19, 9] are dedicated to finding the maximum cut of a graph with weights of the same sign, as the synapses only implement negative weights. The main drawback is that both coupling capacitors and resistors are required to program negative and positive weights, respectively. Other architectures using differential LC oscillators enable signed weights using resistors only [17, 18] but are not scalable on chip due to the bulky LC tanks and resistors. Digital ONNs are promising as they are scalable and modular, as demonstrated by Ahmed et. al. with their 560 ring oscillators chip [11]. A recent promising fully-analog architecture for solving COPs has also been proposed by Graber et. al. [20] that consists of 400 oscillators coupled with nearest neighbors.

1.3 A mixed-signal approach

In this work, we introduce a new mixed-signal ONN architecture, named *Saturated Kuramoto Oscillatory Neural Network* (SKONN) that leverages both analog and digital domains to satisfy the three ONN design criteria. SKONN takes inspiration from the state-of-the-art analog ONN architectures for which the dynamics evolve *naturally* in continuous time and can easily be described by phase models like Kuramoto’s or Izhikevich’s [13], thus facilitating the exploration of potential applications. SKONN’s main novelty consists in setting the computation and propagation in the analog and digital domains, respectively. Fig. 1 illustrates SKONN with 4 fully-coupled neurons. Digital propagation has several advantages such as greater noise immunity, a higher fan-out, and smoother interfacing with other digital circuits. Moreover, the separation between the computation and propagation induces a natural implementation of feed-forward synapses that have never been implemented in literature, to the best of our knowledge.

The paper is organized as follows. First, SKONN architecture is described and its dynamics are derived, highlighting the link between the Kuramoto model and SKONN, and its ability to solve NP-hard Weighted Max-cut problems. Then, we introduce a SKONN-PCB proof-of-concept that solves Weighted Max-cut problems with 9 nodes. A 16-neuron 65nm-ASIC chip recently taped out is also presented, demonstrating SKONN feed-forward ability with a XOR example. Finally, we report on SKONN’s performance scaling in solving the Weighted Max-cut problem, and benchmark with state-of-the-art solvers on G-SET instances.

2 Methods

2.1 SKONN architecture overview

2.1.1 A mixed-signal oscillating neuron

A SKONN neuron consists of a relaxation oscillator producing analog and digital oscillations with period T at its input and output nodes, respectively. Fig.2a shows the block diagram of the oscillating neuron. It consists of a hysteresis circuit that commands a shaper block to charge and discharge a capacitor C_L with constant current I_{bias} . The voltage across the capacitor V_i^{in} is fed back to the hysteresis comparator that switches between V_{DD} and 0 when V_i^{in} reaches the thresholds V_H and V_L , thus producing oscillations. V_i^{out} holds the phase state in the digital domain, whereas V_i^{in} is the analog evolution of the oscillation. Note that the input impedance of the oscillator is purely capacitive in the ideal case so that any charge sent to the input node causes an instantaneous phase shift. The analog waveform V_i^{in} supports the computation and is separated from the digital propagation V_i^{out} , enabling a feed-forward propagation of the phase information.

Fig.2c shows an example of feed-forward propagation between two oscillators. The computation occurs in the analog domain at the input node of neuron i that gathers the output signals from neuron j . The oscillator output signal is a square digital-like signal that carries the oscillator state and evolves until the phase dynamics settle to a fixed point. Choosing a triangular waveform at the analog input leads to simple yet rich phase dynamics that are similar to the Kuramoto model, which is known to have interesting computational properties [13]. Moreover, it skips the use of bulky

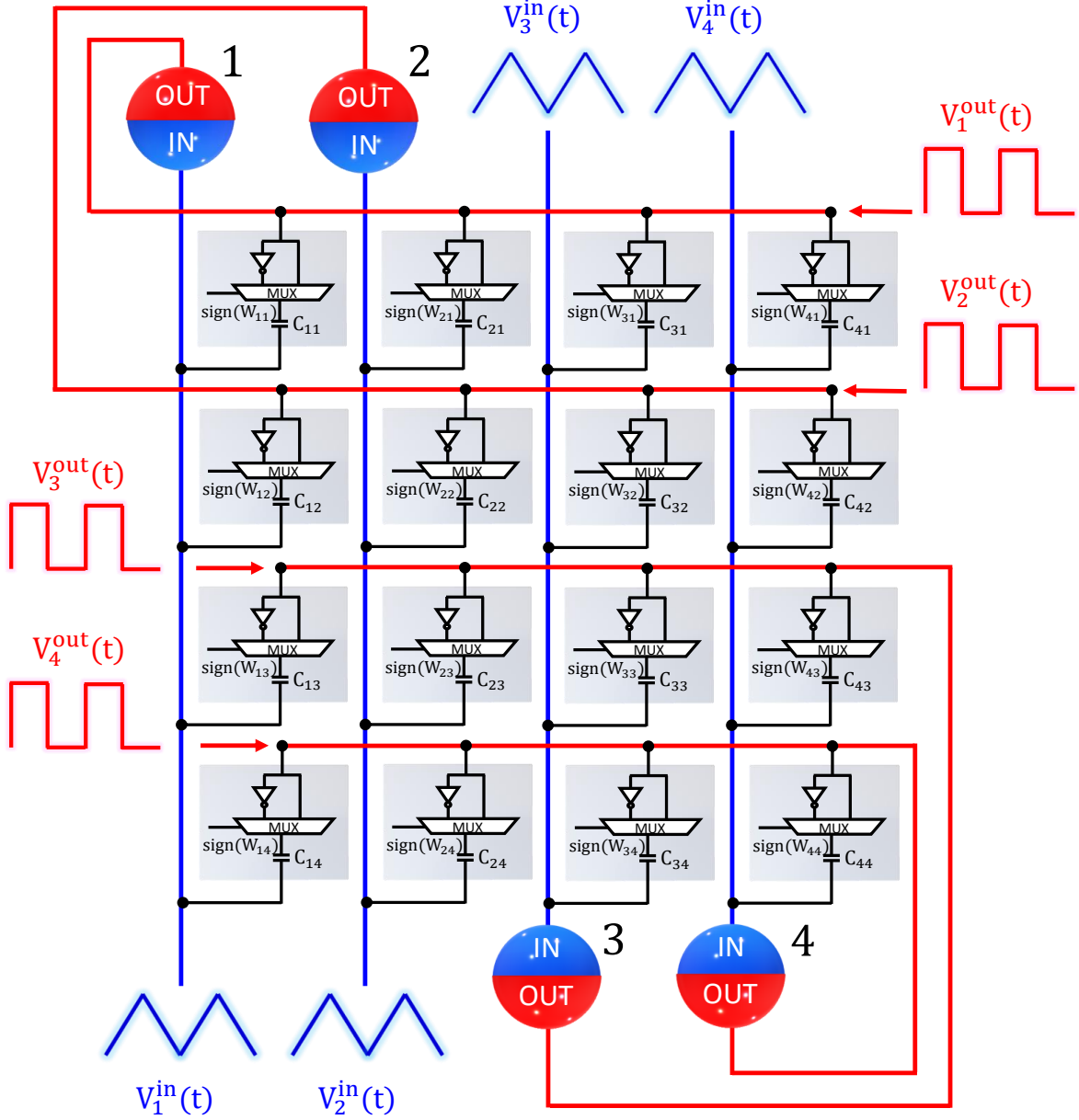


Figure 1: Illustration of a SKONN architecture composed of 4 oscillators and 16 synapses. Neuronal input and output lines are laid out vertically and horizontally, respectively. For neuron i , the input $V_i^{in}(t)$ and output $V_i^{out}(t)$ are synchronized such that $V_i^{out}(t)$ commands the generation of $V_i^{in}(t)$. A synapse S_{ij} consists of a capacitor C_{ij} that converts the digital signal $V_j^{out}(t)$ in current spikes sent to the input node i . The multiplexer sets the weight sign by selecting $V_j^{out}(t)$ or $\overline{V_j^{out}(t)} = V_j^{out}(t - T/2)$. The triangular analog input oscillation $V_i^{in}(t)$ receives the synaptic current spikes, i.e. the charges Q_{ij} , that shift the phase ϕ_i .

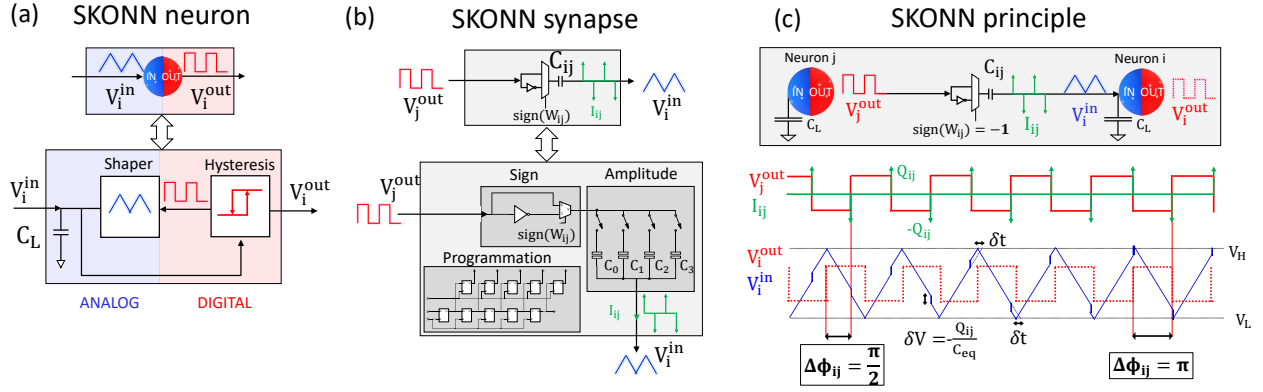


Figure 2: a) The SKONN neuron is a relaxation oscillator composed of two blocks: the hysteresis circuit that holds the neuron state and drives the shaper stage. The latter produces an analog triangular waveform at the input whereas the hysteresis block outputs a digital waveform. b) The SKONN synapse consists of a capacitor bank setting the weight amplitude. A multiplexer selects V_j^{out} or $\overline{V_j^{out}}$ to set the weight sign. c) SKONN principle of computation illustrated with a negative weight. The multiplexer selects $\overline{V_j^{out}}$ that is fed into C_{ij} , creating current spikes I_{ij} aligned with the rising and falling edges of $\overline{V_j^{out}}$. The injected charges $\pm Q_{ij}$ to V_i^{in} induce voltage jumps $\pm \delta V$ that cause time shifts δt . After a few cycles, the two oscillators lock to $\Delta\phi_{ij} = \pi$.

LC tanks needed for producing sinusoidal oscillations. The neuron voltage dynamics are expressed in Appendix A for completeness, although this work rather focuses on phase dynamics that are more suitable to study phase-based ONNs.

2.1.2 Synaptic design and weight sign

A SKONN synapse S_{ij} consists of a capacitor C_{ij} that transmits current pulses, i.e. charges Q_{ij} , from the output of oscillator j to the input of oscillator i . C_{ij} can easily be programmed using a capacitor bank and a register, as shown in Fig. 2b. Instead of propagating the sensitive analog signal, SKONN only transmits the oscillator phase information in a robust manner. The digital output voltage V_j^{out} is applied to C_{ij} that creates current spikes holding the phase information ϕ_j . The synaptic spike train can be expressed as follows:

$$I_{ij} = C_{ij} \left(\frac{dV_j^{out}}{dt} - \frac{dV_i^{in}}{dt} \right) \quad (1)$$

The synaptic capacitor can be thought of as a digital-to-analog phase converter. The synaptic weight consists of the capacitance value C_{ij} that linearly modulates the charge sent to the oscillating input node i as $Q_{ij} = C_{ij}V_{DD}$, thus inducing phase shifts in the oscillation i as shown in Fig.2c. To implement a negative weight, the complementarity of V_j^{out} defined as $\overline{V_j^{out}}(t) = V_j^{out}(t - T/2)$ is selected using a multiplexer and applied to C_{ij} . Compared to resistors, synaptic capacitors have several advantages for upscaling the ONN:

1. ONN computation models are generally based on the weak coupling assumption [13, 8] and necessitate weak synaptic signals. This means the ONN needs either large coupling resistors or small capacitors, the latter being much more scalable in a chip.
2. For a limited neuron output strength, the only way of increasing the synaptic fan-out is to reduce the synaptic current, which again would lead to bulky resistors or smaller capacitors in the case of SKONN.

2.2 SKONN phase dynamics

2.2.1 2 coupled oscillators

SKONN computing mechanism is illustrated in Fig.2c with the case of a neuron j feeding its phase to another neuron i in a feed-forward manner with a negative weight. This means that $\overline{V_j^{out}}$ is selected by the multiplexer and applied to C_{ij} , thus creating current spikes $+Q_{ij}\delta(t)$ and $-Q_{ij}\delta(t - T/2)$ that are aligned with the rising and falling edges of $\overline{V_j^{out}}$, respectively. Each injected charge $\pm Q_{ij}$ induces a voltage jump $\delta V = \pm Q_{ij}/C_{eq}$ at the input node, with

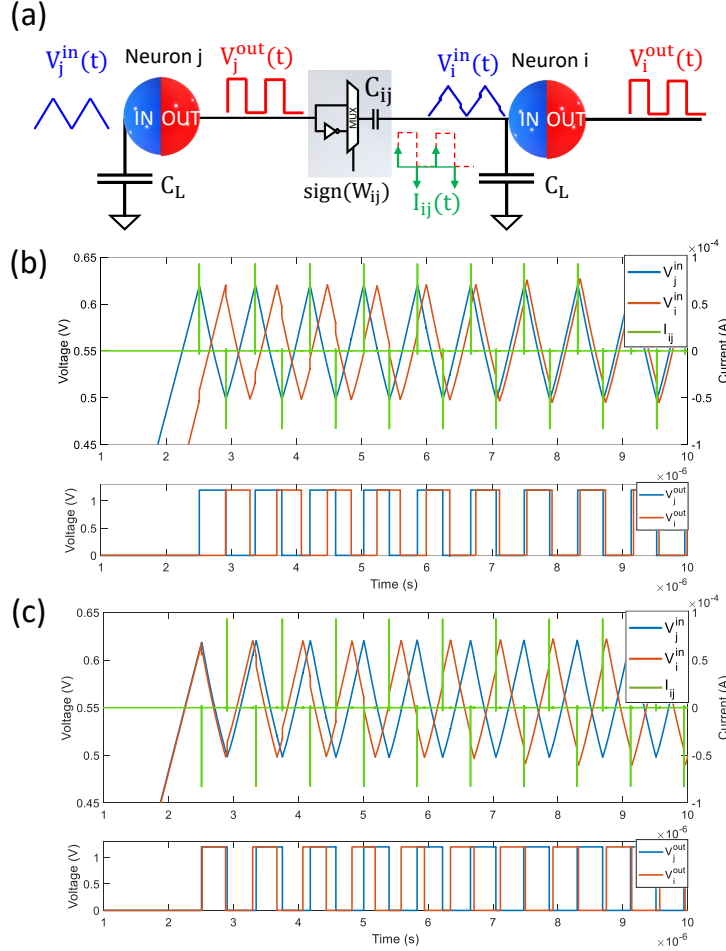


Figure 3: (a) Illustration of a neuron that drives a second neuron in a feed-forward manner. The multiplexer sets the weight sign and the capacitor C_{ij} converts the digital signal $V_j^{out}(t)$ into current spikes $I_{ij}(t)$ that induce phase shifts of the input $V_i^{in}(t)$. (b) Transistor-level transient simulation with a positive weight $W_{ij} > 0$. The second phase catches up the first one after few cycles such that $\Delta\phi_{ij} \approx 0^\circ$. (c) Simulated dynamics with a negative weight $W_{ij} < 0$. The second phase is pushed such that $\Delta\phi_{ij} \approx 180^\circ$ after few cycles.

$C_{eq} = C_L + C_{ij}$. As V_i^{in} is a triangular waveform, δV provokes a time shift $\delta t = \pm C_{eq} \delta V / I_{bias}$, where \pm indicates here the sign of V_i^{in} 's slope. Knowing the period of the triangular oscillation $T = 2C_{eq} \Delta V / I_{bias}$ where ΔV is V_i^{in} 's peak-to-peak amplitude, we can then express the phase shift related to a single current spike:

$$\begin{aligned}
 \delta\phi &= 2\pi \frac{\delta t}{T} \\
 &= \pi \frac{\pm Q_{ij}}{C_{eq} \Delta V} \\
 &= \pi \frac{\pm C_{ij}}{C_{eq}} \frac{V_{DD}}{\Delta V} \\
 &\approx \pi \frac{\pm C_{ij}}{C_L} \frac{V_{DD}}{\Delta V} \quad \text{if } C_L \gg C_{ij}
 \end{aligned} \tag{2}$$

SKONN's unique feature consists of this simple relation (2) between coupling capacitors and phase shift, thus enabling well-controlled phase dynamics and a precise weight mapping to the coupling capacitor C_{ij} . As we will see later, the quantity $\beta_0 = |\delta\phi / Q_{ij}|$ provides the neuron phase sensitivity with respect to the charge perturbation. It is linked to the

Phase Perturbation Vector (PPV) of the oscillator which is key for deriving SKONN's phase dynamics [32]. SKONN's PPV is defined and derived in Appendix B.

Two coupled oscillators converge either in- or out-of-phase, depending on the synaptic sign. To show this property, we use SKONN's phase dynamics that are derived in Appendix C using the PPV formalism [32]. Under the weak coupling assumption ($C_{ij} \ll C_L$), the phase dynamics of oscillator i can be expressed as follows:

$$\frac{d}{dt}\phi_i = 2\beta_0 \frac{Q_{ij}}{T} \text{square}(\phi_i - \phi_j) \quad (3)$$

With the 2π -periodic function

$$\text{square}(\theta) = \begin{cases} -1, & \text{if } 0 < \theta < \pi \\ +1, & \text{if } \pi < \theta < 2\pi \end{cases} \quad (4)$$

The phase fixed points can be derived from (3) and are expressed in the next proposition.

Proposition 1. *If the injected charge $Q_{ij} \neq 0$ then the two SKONN oscillators admit a unique stable fixed-point $\Delta\phi^* = (\phi_i - \phi_j)^*$ such that*

$$\Delta\phi^* = \begin{cases} 0, & \text{if } Q_{ij} > 0 \\ \pi, & \text{if } Q_{ij} < 0 \end{cases} \quad (5)$$

The proof is shown in Appendix C. In other words, propagating a spike train defined as (1) induces an in-phase or out-of-phase locking, depending on the polarity of Q_{ij} . Each current spike produces a local phase shift to the analog input oscillation, resulting in an average phase shift $\Delta\phi = \pm 2\beta_0 Q_{ij}$ after each cycle (3). Fig.3b shows a transistor-level simulation of the positive weight case. I_{ij} perturbs V_i^{in} until the oscillators converge in phase. Similarly, Fig.3c shows the same configuration with a negative weight and the oscillators are out-of-phase.

Note that the phases measured from the rising edges of V_i^{out} and V_j^{out} are slightly shifted from the theoretical fixed points (5). This is mainly due to the limited bandwidth of the hysteresis block which does not switch instantaneously when reaching its thresholds. This non-ideality can be compensated and is further discussed in Appendix E. Interestingly, this phase shift disappears with symmetric synapses as both oscillators are equally delayed (see Fig.6c).

2.2.2 N coupled oscillators

The phase dynamics of N sinusoidal coupled oscillators are often expressed using the Kuramoto model [13, 15, 8]:

$$\frac{d}{dt}\phi_i = -\omega_0 \sum_{j=1}^N K_{ij} \sin(\phi_i - \phi_j) \quad (6)$$

Where ω_0 is the frequency in rad/s and K_{ij} the coupling coefficients. Similarly, we derive SKONN's phase dynamics for N oscillators as follows:

$$\frac{d}{dt}\phi_i = \omega_0 \frac{V_{DD}}{\Delta V} \sum_{j=1}^N \frac{C_{ij}}{C_L} \text{square}(\phi_i - \phi_j) \quad (7)$$

Where we replaced β_0 and Q_{ij} from (3) by their expressions $\beta_0 = \pi/(\Delta V C_L)$ and $Q_{ij} = C_{ij} V_{DD}$. The derivation is detailed in Appendix C. V_{DD} is the digital voltage swing, ΔV is the peak-to-peak triangular voltage amplitude at the input, C_{ij} is the synaptic capacitance value, and C_L is the neuron input capacitance.

SKONN's phase dynamics are very similar to the Kuramoto model (6) except for its sinusoidal function replaced by a *saturated* square function in this work. It induces a binarization behavior that is useful for solving some optimization problems as shown later.

Proposition 2. *Consider a neuron i of degree D , i.e. driven by D neurons j with weighted charges $Q_{ij} \in \{-q, +q\}$ $q \neq 0$.*

1. *If D is odd and $d\phi_i/dt = 0$, then there is at least one input neuron j such that $(\phi_i - \phi_j)$ is a multiple of π .*
2. *If D is even, then there is at least one ϕ_i and one set of input phase ϕ_j such that $d\phi_i/dt = 0$ and $\forall j$ $(\phi_i - \phi_j)$ is not a multiple of π .*

The proof is shown in Appendix C. Interestingly, odd-degree neurons will phase-lock in- or out-of-phase with at least one input phase. The odd-degree property will be advantageous for solving some optimization problems on graphs,

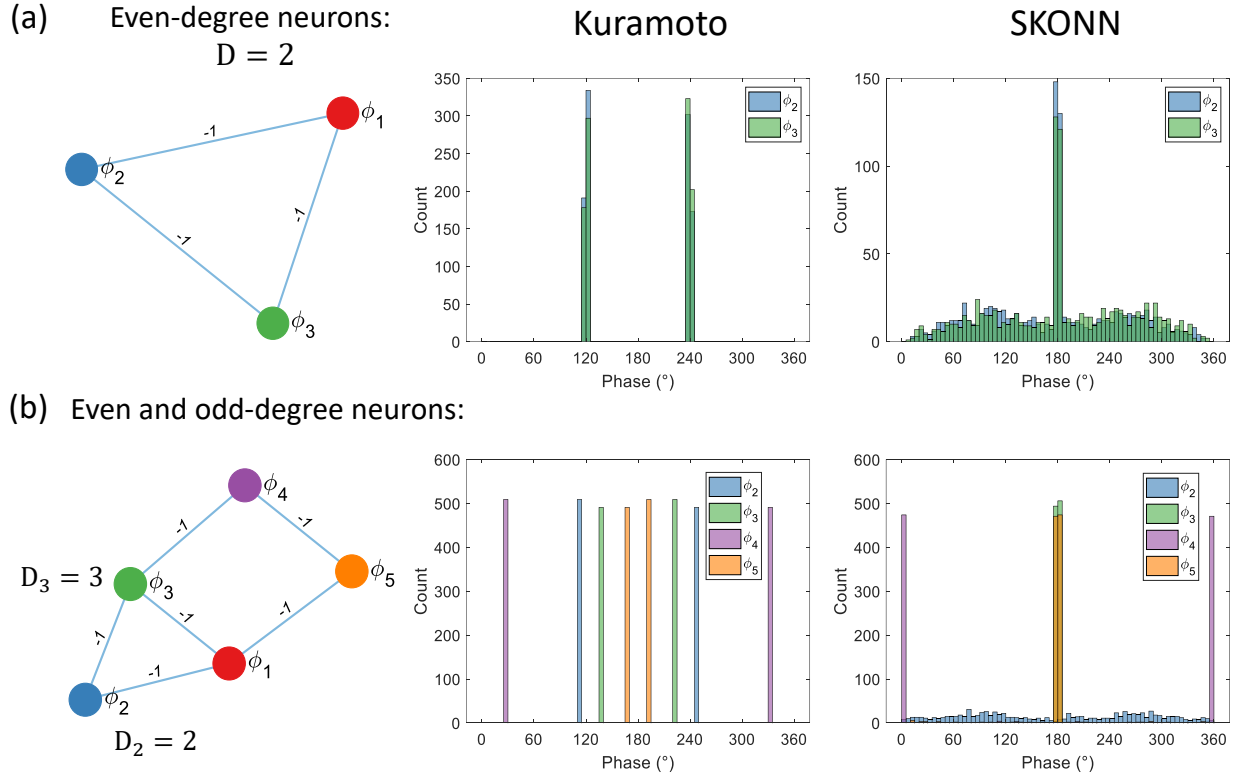


Figure 4: a) Three oscillators coupled by negative weights. The right-hand-side plots show the Kuramoto and SKONN distributions of the final phases for 1000 random initializations (uniform distribution). The Kuramoto-ONN converges to two fixed points $(\phi_2^*, \phi_3^*)=(120^\circ, 240^\circ)$ or $(\phi_2^*, \phi_3^*)=(240^\circ, 120^\circ)$. Whereas SKONN phases can settle to various analog phases as each oscillator has an even number of input synapses D . b) Five coupled oscillators where D_1, D_3 and D_2, D_4, D_5 are odd and even, respectively. The Kuramoto-ONN settles to two fixed points $(\phi_2^*, \phi_3^*, \phi_4^*, \phi_5^*) \approx (248^\circ, 137^\circ, 331^\circ, 166^\circ)$ or $(\phi_2^*, \phi_3^*, \phi_4^*, \phi_5^*) \approx (112^\circ, 223^\circ, 29^\circ, 194^\circ)$. SKONN tends to binarize phases except ϕ_2 that can rather converge to any phase value.

as shown in the section 3.4. On another hand, an even number of inputs rather leads to a relaxed scenario where the neuron can settle into an infinite number of phases and could prevent phase binarization.

For instance, Fig.4a shows a graph implemented with three fully-connected neurons with $D=2$. In this simulation, we randomly initialized the phases, numerically solved (7) and measured the final phases with respect to the reference ϕ_1 . It can be seen from the distribution of final phases for 1000 trials that SKONN can settle to arbitrary analog phases, whereas the Kuramoto-ONN always converges to a single phase fixed point $\phi^*=(0^\circ, 120^\circ, 240^\circ)$. When SKONN has both odd and even numbers of input synapses, we heuristically find that most of phases tend to binarize as illustrated with the 5-node graph in Fig. 4b, although some phases (such as ϕ_2) can still converge to fixed points with arbitrary phase values. This aspect will be further discussed when solving larger graphs in section 3.4.

Note that similar dynamics have already been explored in simulation by Wang et. al. in their work about Oscillatory Ising Machines (OIM) [8]. The authors studied the case where the sinusoidal term $\sin(\Delta\phi)$ from Kuramoto (6) is replaced by $\tanh(\alpha \sin \Delta\phi)$ with $\alpha = 10$. As SKONN's square interaction can be thought as $\text{square}(\Delta\phi) \approx -\tanh(\alpha \sin \Delta\phi)$ for $\alpha \gg 1$, we expect SKONN to have good performances when solving NP-hard combinatorial optimization problems.

2.3 SKONN energy landscape

SKONN stability can be proved by applying the Convergence Theorem for Oscillatory Neural Networks derived by Hoppensteadt and Izhikevich [35]. With an odd coupling function (4) and symmetric coupling $Q_{ij} = Q_{ji}$, the theorem ensures that the phase differences converge to a stable fixed point. The proof consists of finding a Lyapunov function for the dynamics (7) that is bounded below and minimized through time. A candidate for the SKONN Lyapunov function

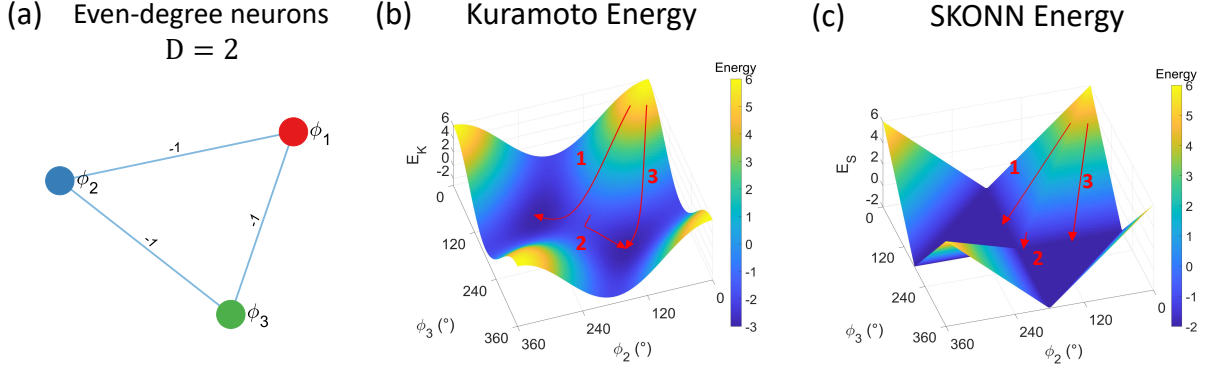


Figure 5: a) Three oscillators coupled by negative weights. b) and c) Corresponding Kuramoto and SKONN energy landscapes, respectively. The arrows represent three examples of trajectories with various initializations, highlighting Kuramoto's minima and saddle point. In this example, SKONN's energy minima consist of plateaus that are linked to the even-degree property (Proposition 2.2).

is:

$$E = \frac{\beta_0}{T} \sum_{i,j}^N Q_{ij} \text{triangle}(\phi_i - \phi_j) \quad (8)$$

With:

$$\text{triangle}(\theta) = \begin{cases} \theta - \pi/2, & \text{if } 0 \leq \theta \leq \pi \\ 3\pi/2 - \theta, & \text{if } \pi \leq \theta \leq 2\pi \end{cases} \quad (9)$$

Under the assumption that $Q_{ij} = Q_{ji}$, one can check that:

$$\begin{aligned} \frac{\partial E}{\partial \phi_k} &= \frac{\beta_0}{T} \left(- \sum_{j=1}^N Q_{kj} \text{square}(\phi_k - \phi_j) \right. \\ &\quad \left. + \sum_{i=1}^N Q_{ik} \text{square}(\phi_i - \phi_k) \right) \\ &= - \frac{d\phi_k}{dt} \end{aligned} \quad (10)$$

Thus, SKONN minimizes E over time:

$$\begin{aligned} \frac{dE}{dt} &= \sum_{k=1}^N \frac{\partial E}{\partial \phi_k} \frac{d\phi_k}{dt} \\ &= - \sum_{k=1}^N \left(\frac{d\phi_k}{dt} \right)^2 \leq 0 \end{aligned} \quad (11)$$

SKONN's and Kuramoto's energy landscapes are represented for the three fully-coupled oscillators case in Fig.5. We observe that SKONN's energy landscape has two plateaus where the phases can settle and remain stable, which is consistent with the phase distribution from Fig.4a and linked to the even number of synaptic inputs (Proposition 2.2). Whereas the Kuramoto energy landscape consists of two minima and a saddle point, as highlighted by the three simulated trajectories of Fig.5b and c. Unfortunately, we cannot visualise the energy landscape for larger networks but a local analysis around a phase fixed point can reveal the landscape around it (discussed in the supplementary material). There can be sharp hills in some directions and plateaus in others. For instance in the 5-node case of Fig.4b, most of the fixed points are surrounded by hills in all directions except for the direction ϕ_2 which consists of a trench where E remains constant.

So far, we have seen that SKONN has simple yet rich phase dynamics with unique phase binarization properties resumed in Proposition 2. Moreover, SKONN's phase evolution can be interpreted as the minimization of a N-dimensional

energy landscape E (8) and thus naturally performs the gradient descent of E through time. One can harness this concept for solving optimization problems that consist in finding minima of a cost function. In the next sections, we focus on the NP-hard Max-cut problem and present two approaches for solving Max-cut with SKONN.

2.4 SKONN for solving the NP-hard Max-cut problem

Given a graph with a set V of N vertices connected by weighted edges $W_{ij} = W_{ji}$, the Max-cut problem consists in *cutting* the graph in two complementary subsets of vertices V_1 and V_2 such that the sum of weights between V_1 and V_2 is maximum. The Max-cut problem can be formulated as follows [36]:

$$\begin{aligned} & \text{Max} \frac{1}{2} \sum_{i,j} W_{ij} (1 - S_i S_j) \\ & \text{subject to:} \\ & S_i \in \{-1, +1\} \forall i \in V \end{aligned} \tag{12}$$

Solving the Max-cut problem is NP-hard and the best-known approximation algorithm is the Semidefinite Programming (SDP) algorithm found by Goemans and Williamson [36] and denoted GW throughout the paper. By relaxing the binary spins S_i to unit vectors v_i in \mathbb{R}^N , GW relaxes the NP-hard Max-cut problem to an SDP convex problem for which optimality can be found in polynomial time:

$$\begin{aligned} & \text{Max} \frac{1}{2} \sum_{i,j} W_{ij} (1 - v_i \cdot v_j) \\ & \text{subject to:} \\ & v_i \in \mathbb{R}^N \\ & |v_i| = 1 \forall i \in V \end{aligned} \tag{13}$$

To compute the cut, the vectors are finally assigned to binary spins by splitting in two the N-dimensional sphere with a random hyper plan. Repeating this final rounding step provides a cut at least 0.878 times the maximum cut in expectation. However, due to the high dimension of the problem relaxation (\mathbb{R}^N), GW is costly for large instances [37, 38] and alternative approaches using physical systems such as Quantum Annealers [39], coherent Ising machines [38], memristors [40] or coupled oscillators are being investigated [8, 11, 9, 19].

2.4.1 The Ising approach

One of the most studied formalisms applied to ONN is from Ising which was initially derived to study magnetism in materials [41]. Given interaction coefficients $J_{ij} \in \mathbb{R}$ between particles that can have two spins $S_i \in \{-1; +1\}$, the particles relax to a state that minimizes the Ising Hamiltonian (we skip the external fields for simplicity):

$$H = -\frac{1}{2} \sum_{i,j} J_{ij} S_i S_j \tag{14}$$

Thanks to Lucas' seminal work [42], all Karp's 21 NP-complete problems can be mapped to the Ising formalism and the solutions can be approximated by any physical machine that minimizes the Ising Hamiltonian (14). If SKONN phases take binary values $\phi_i = (1 - S_i)\pi/2 \in \{0, \pi\}$, its Lyapunov function (8) becomes:

$$\begin{aligned} E &= \frac{\beta_0}{T} \sum_{i,j} Q_{ij} \text{triangle}\left(\frac{\pi}{2}(S_j - S_i)\right) \\ &= -\frac{\pi\beta_0}{2T} \sum_{i,j} Q_{ij} S_i S_j \\ &\propto H \end{aligned} \tag{15}$$

Each synaptic current spike can be thought of as a downward step (due to equation (11)) in the energy landscape (8) which corresponds to the Ising Hamiltonian (15) if the final phases are binary. However, having binary phases is not guaranteed in general as we have seen with the Proposition 2.2. To force phase binarization, it is common practice to inject into the oscillators a SHIL periodic signal at twice the oscillating frequency [8] and described in Appendix D for SKONN.

The Max-cut problem can easily be mapped to an Oscillatory Ising Machine (OIM) with spins corresponding to the graph vertices by setting $J_{ij} = -W_{ij}$ with W_{ij} the graph weights [42]. Then, the OIM performs the following minimization which is equivalent to the Max-cut (13):

$$\begin{aligned} \text{Min } H &= \text{Max} \left(-\frac{1}{2} \sum_{i,j} W_{ij} S_i S_j \right) \\ \text{subject to:} & \\ S_i &\in \{-1, +1\} \forall i \in V \end{aligned} \tag{16}$$

The general strategy is to 1) map the graph to the OIM, 2) start the OIM while ramping up a 2-SHIL signal to binarize the phases, and 3) read the stable phase state [8]. Forcing phase binarization is common practice as it maps the OIM Lyapunov function to the Ising Hamiltonian (15). However, how to binarize is not straightforward. If the injected signal is too strong, it may "freeze" the phases to sub-optimal local minima [8]. Whereas if the signal is too weak, it might increase the OIM computation time. In this work, we rather harness the free SKONN dynamics without SHIL to compute the Max-cut.

2.4.2 A Rank-2 relaxation approach

Erementchouk et. al. [43] have recently shown that the free OIM relaxation can be harnessed to solve the Max-cut problem. Their recent results demonstrate that letting a Kuramoto-ONN settle to analog phase values is equivalent to solving a rank-2 relaxation problem for the NP-hard Max-cut problem. Such phase dynamics are used in the CirCut solver [37]. Similarly to GW, the CirCut algorithm relaxes spins S_i to 2D unit vectors $x_i \in \mathbb{R}^2$ such that $x_i = (\cos(\phi_i) \sin(\phi_i))$ that can take arbitrary values on the unit circle. The objective of the rank-2 relaxation is:

$$\begin{aligned} \text{Max } &\frac{1}{2} \sum_{i,j} W_{ij} (1 - x_i \cdot x_j) \\ &= \text{Max } \frac{1}{2} \sum_{i,j} W_{ij} (1 - \cos(\phi_i - \phi_j)) \\ \text{subject to:} & \\ x_i &\in \mathbb{R}^2 \\ |x_i| &= 1 \forall i \in V \end{aligned} \tag{17}$$

Then, a rounding procedure produces spins to compute the graph cut. Unfortunately, this rank-2 algorithm cannot guarantee a lower bound on the cut as it remains a non-convex optimization problem. Nevertheless, its accuracy is comparable to the GW algorithm in practical use [37]. In this paper, we only explore the relaxation approach where we let SKONN settle without forcing binarization. We will see that SKONN's phase binarization property (Proposition 2.1) is particularly useful in this case. For the Ising approach, we invite the reader to consult the excellent work from Wang and Roychowdhury [8] as the reported dynamics are equivalent to SKONN's.

3 Results

3.1 3x3 SKONN PCB

We designed a 3x3 SKONN on PCB with fully-connected capability and 81 synapses (Fig.6a) as a proof of concept for the SKONN architecture. Due to area constraints, we only implemented negative weights that we program by placing discrete capacitors C_{ij} manually. Fig.6b shows the oscillating neuron based on a Schmitt trigger (U1) with feedback resistor R_3 that charges/discharges a load capacitor C_L , producing a triangular-like waveform with 720 mVpp amplitude. The neuron output is a square-like waveform oscillating between $V_{DD} = +0.9\text{V}$ and $V_{SS} = -0.9\text{V}$. Using an FPGA, we set the initial phase state by delaying the oscillator's starting time (Q1). The FPGA measures the neurons' output voltages and allows phase post-processing with a maximum precision of $\epsilon = 360^\circ f_0 / f_{FPGA}$. In our experiments we set $f_0 = 4\text{kHz}$, $f_{FPGA} = 50\text{MHz}$ and $\epsilon \approx 0.03^\circ$.

Fig.6c shows an experiment of two oscillators weakly coupled by $C_{12} = C_{21} = 1\%C_L$ whereas Fig.6d is a strong coupling with $C_{12} = C_{21} = 10\%C_L$. In both experiments, the oscillators are out-of-phase but the strong coupling case leads to a frequency reduction of -34% as the voltage jumps $\Delta V = (V_{DD} - V_{SS})C_{12}/C_L$ produced by each current spike are too large with respect to the analog amplitude. This phenomenon can induce frequency mismatches between groups of strongly coupled oscillators and groups of weakly coupled oscillators. Frequency mismatches still need to be investigated and here we empirically choose $C_{ij} < 5\%C_L$ to guarantee phase locking among oscillators.

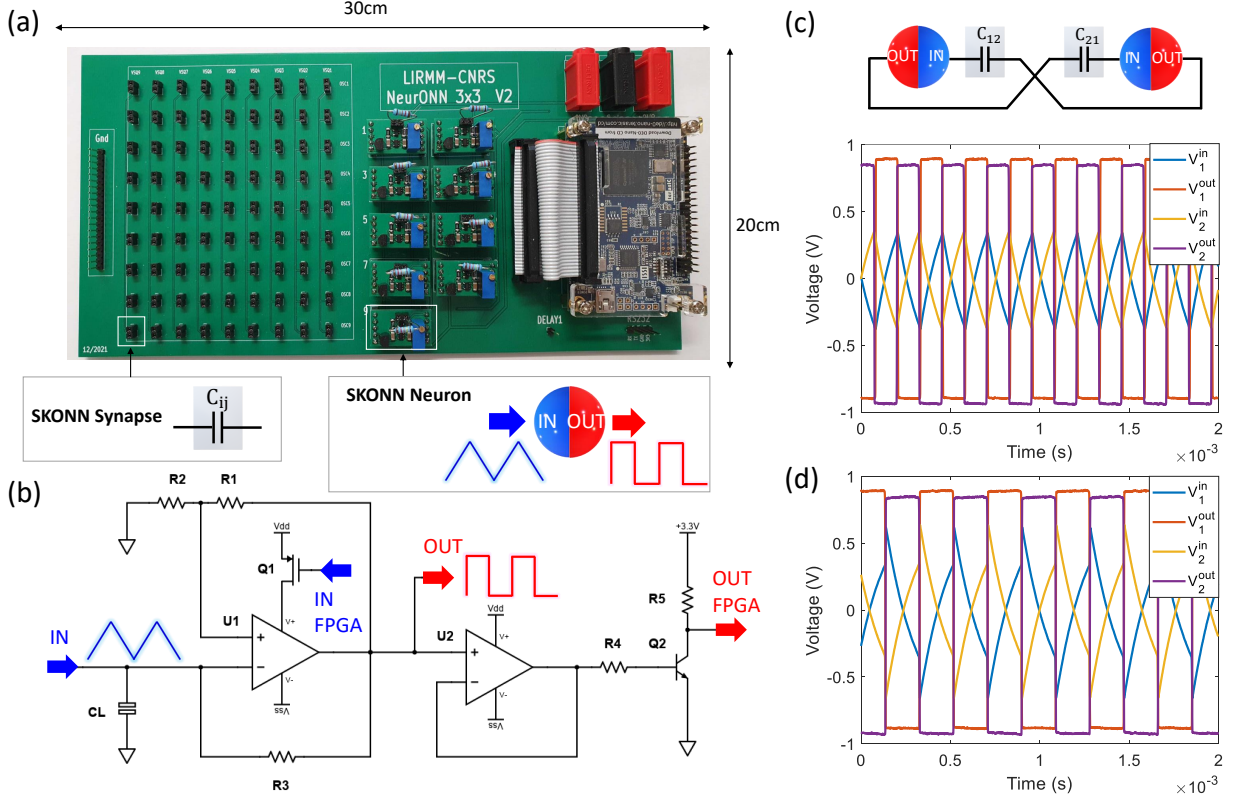


Figure 6: (a) SKONN on PCB with 9 oscillators and 81 synapses. We set the weight amplitude with the synaptic capacitance value C_{ij} . The FPGA initializes the phases by delaying the oscillators' starting time by switching Q1 and measures the digital oscillations buffered by the output stage (U2 and Q2). (b) The oscillator consists of a OP-amp Schmitt trigger feedback by the resistor R_3 to produce self-oscillations. $R_1//R_2$ sets the analog oscillation amplitude. (c) Two coupled oscillators with $C_{12}/C_L = C_{21}/C_L = 1\%$. (d) Two coupled oscillators with $C_{12}/C_L = C_{21}/C_L = 10\%$.

3.2 Weighted Max-Cut on PCB

The test case consists of the Max-cut problem with 2-bit positive weights. We generate random instances of Erdos-Rényi graphs $G(N, p)$ [44] with $N=9$ nodes and p is the probability to have an edge between a pair of vertices such that the total number of edges $m = pN(N-1)/2$. For each graph edge, the weight is randomly selected from the list $[0\ 10\ 22\ 47]/47$ that corresponds to discrete capacitors used experimentally.

Fig.7a shows an example of a dense random graph instance with $p = 0.75$. We map the graph edges to the synaptic matrix and run 100 trials with random phase initializations. For each trial, the nine phases are sampled every oscillation period during 1000 oscillation cycles. Fig.7b shows the final phases $\phi_i(t = 1000T)$ measured for each trial, the latter indicated as the amplitude in the polar plot. The right-hand side of the polar plot corresponds to positive spins, whereas the left-hand side corresponds to negative spins. It appears that some phases such as ϕ_2 , ϕ_4 and ϕ_6 are always assigned to the same spin polarity whereas most of the phases can end up in both half-circles, depending on the phase initialization. Hence, SKONN final states depend on the initialization and several trials ensure obtaining a good solution. Fig.7c shows the histogram of solution and the settling time. SKONN finds the graph Max-cut with 75% probability in less than 100 oscillation cycles on average. Fig.8 presents another Weighted Max-cut problem with $G(9, 0.5)$. Other Max-cut examples are shown in the supplementary material file.

3.3 4x4 SKONN CMOS design

3.3.1 SKONN Integrated Circuit

To further assess SKONN performances, we taped out an ASIC chip using a 65nm technology. Fig.9a shows the chip layout view and Table 2 contains the chip specifications. For this first ASIC version, we have focused on transistor

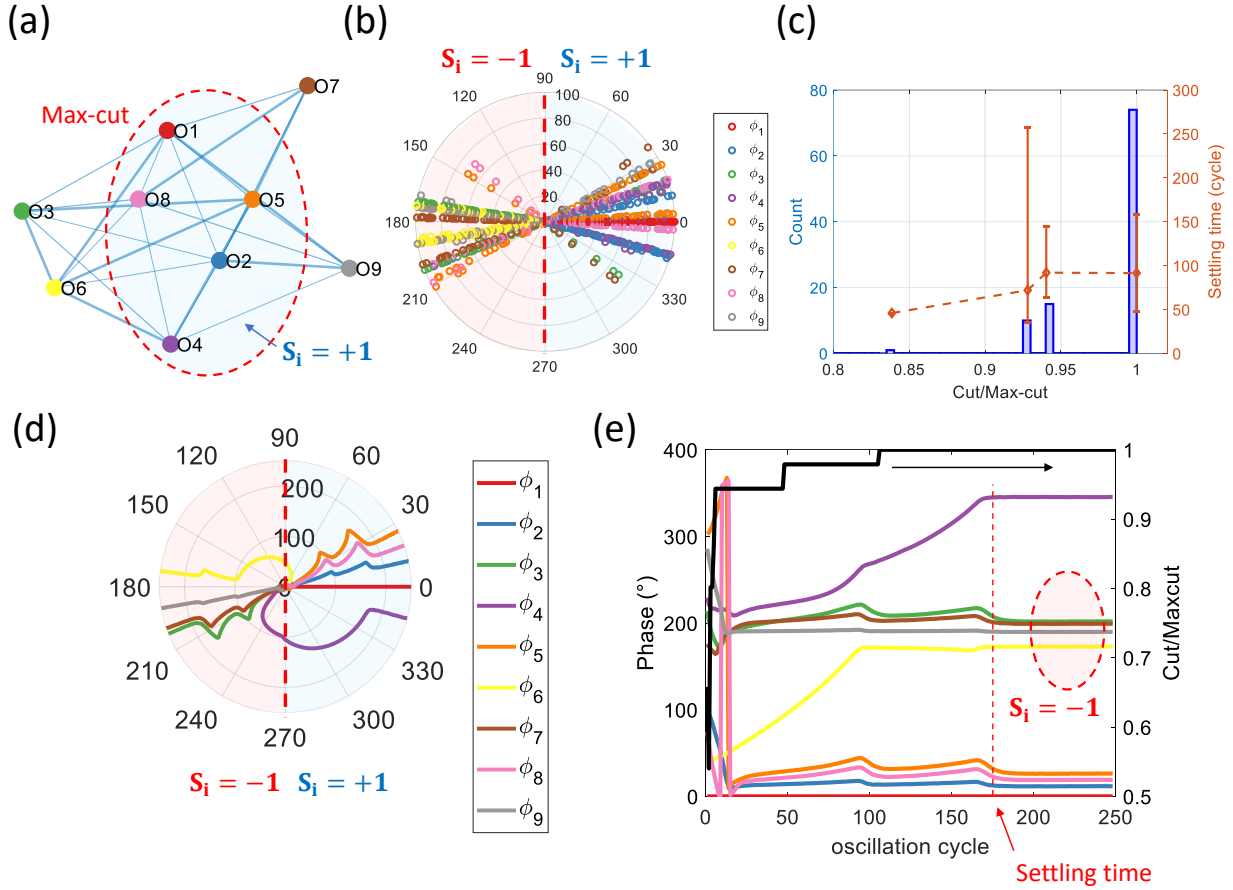


Figure 7: (a) Random instance of $G(9, 0.75)$ with 2-bit weighted edges. (b) Phases measured after 1000 oscillation cycles. The polar amplitude represents the trial number (100 trials). We assign $-90^\circ < \phi_i < 90^\circ \rightarrow S_i = +1$ and $90^\circ \leq \phi_i \leq 270^\circ \rightarrow S_i = -1$. (c) Histogram of Max-cut solutions for 100 trials and measured settling time. (d) Example of phase dynamics in polar representation. The polar amplitude corresponds to the time expressed in cycles. (e) Same dynamics represented in Cartesian plot with the cut evolution.

matching to minimize the variations among oscillators and enhance the robustness. The second main objective was a low power consumption ($160 \mu\text{W}$ without IOs). Although there are 16x more synapses than neurons, the synapses represent only 20% of the power consumption and are promising for solving dense networks. The constraint on the oscillator matching led to a large oscillator area ($5000 \mu\text{m}^2$) but could be overcome with some calibration technique. Although the total chip area is 3.9 mm^2 , there is room for improvement as the core area is 1.1 mm^2 , and 71% of the total area consists of routing lines from the core to the high number of IOs and test pads (90).

Similarly to the SKONN design on PCB, the oscillating neuron consists of a hysteresis regenerative comparator whose digital output drives the charge and discharge of the capacitor $C_L=500\text{fF}$ in the shaper block (Fig.9d). The comparator switches whenever the input voltage V_i^{in} reaches one of the two voltage thresholds V_H and V_L that define the analog voltage amplitude as $\Delta V = V_H - V_L = 120 \text{ mV}$ and $(V_H + V_L)/2 = V_{REF}=600 \text{ mV}$. The synaptic block consists of a capacitor bank ranging from 0 to 37.5fF that linearly maps the weight amplitude from 0 to 15 ($C_0 = C_1/2 = C_2/4 = C_3/8=2.5\text{fF}$). The weight sign is selected by the multiplexer commanded by the sign bit B_S . The synaptic matrix is programmed by sending serially the $5 \times 256=1280$ bits through the registers.

Table 3 presents the specifications of the state-of-the-art ONNs designed using CMOS technology. The connectivity scheme can be all-to-all for small-sized ONNs ($N \leq 100$) but is obviously reduced to nearest neighbor connections for larger ONNs such as in [11] and [20] that chose to connect 6 and 8 (King's graph) neighbors, respectively. SKONN's input/output separation allows any type of modular connectivity in a robust manner as the synaptic signal from 2-coupled

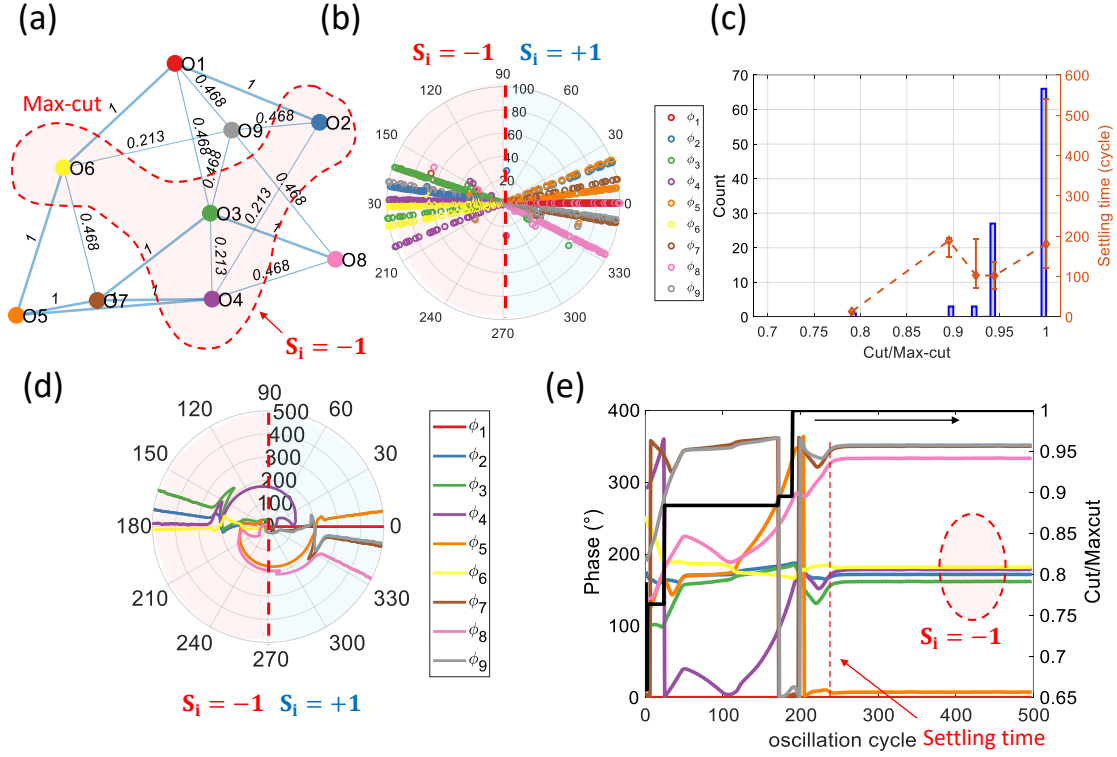


Figure 8: (a) Random instance of $G(9, 0.5)$ with 2-bit weighted edges. (b) Phases measured after 1000 oscillation cycles. The polar amplitude represents the trial number (100 trials). We assign $-90^\circ < \phi_i < 90^\circ \rightarrow S_i = +1$ and $90^\circ \leq \phi_i \leq 270^\circ \rightarrow S_i = -1$. (c) Histogram of Max-cut solutions for 100 trials and measured settling time. (d) Example of phase dynamics in polar representation. The polar amplitude corresponds to the time expressed in cycles. (e) Same dynamics represented in Cartesian plot with the cut evolution.

Table 2: SKONN ASIC specifications

Technology	Neurons	Synapses	Synaptic precision	f_{osc}	SHIL inputs	Area	Power
65nm	16	256	5 bits	1-4 MHz	16	3.9 mm ² Neurons: 2 % Synapses: 24 % Biasing: 3 % Routing, IOs: 71 %	160 μ W Neurons: 75 % Synapses: 20 % Biasing: 5 %

oscillators cannot leak to any other oscillator. This contrasts with fully-analog architectures such as [19, 9] that merge input/output nodes, resulting in undesired current paths between non-adjacent oscillators. It appears that digital ONNs such as [5] and [11] are very energy-efficient as they produce a single oscillation with only 300 fJ. In contrast, analog oscillators found in [20] and this work consume 2.3 pJ and 10 pJ per oscillation, respectively. However, we believe that SKONN's energy could be reduced by relaxing the constraints on the analog oscillator matching and using a calibration scheme instead, as proposed by Graber et. al. [20].

3.3.2 Feed-Forward Network with SKONN

Propagating the information in a feed-forward manner is useful in some applications that require driving neurons. For instance, when training an ONN with the Equilibrium Propagation method [45, 46], one must nudge the output

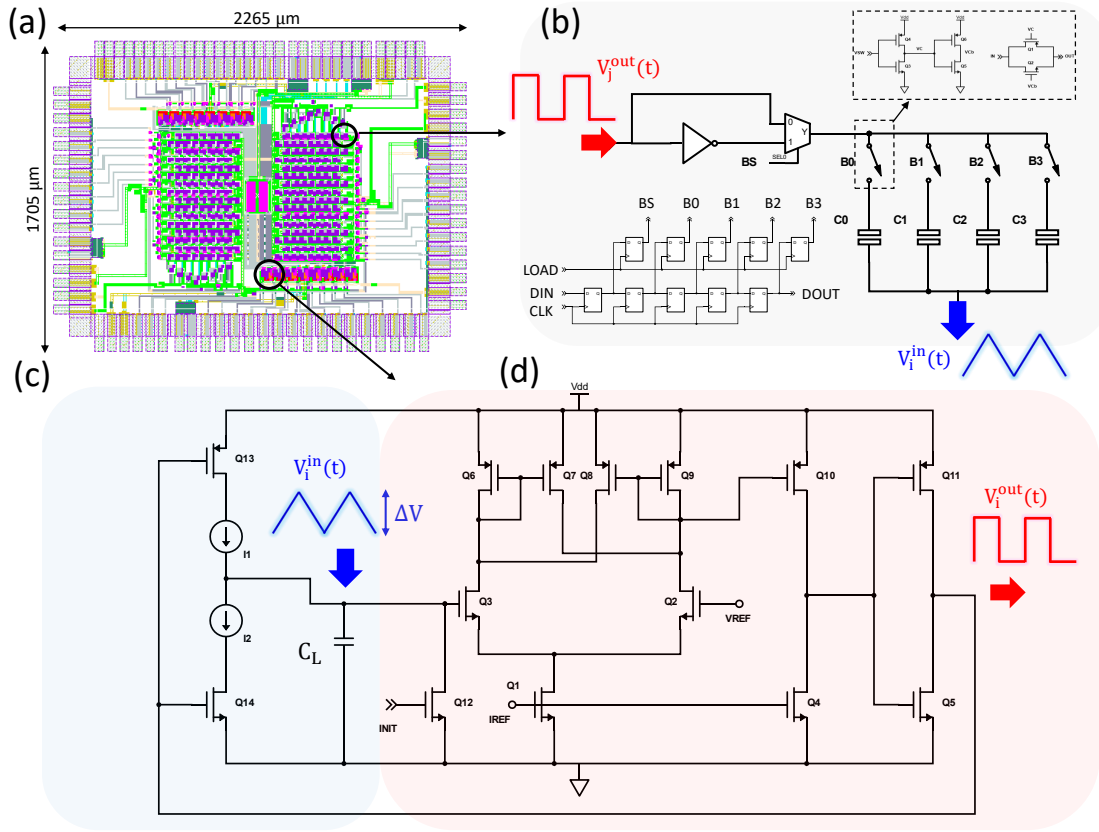


Figure 9: a) Layout view of the taped out SKONN ASIC. There are 16 neurons and 256 synapses laid out as in Fig.1. b) SKONN synapse with 5 bits precision. The four parallel capacitors set the the weight amplitude from 0 to 15. The bit B_S selects the weight sign from the multiplexer. c) Shaper circuit producing the input triangular oscillation. d) Regenerative comparator that holds the neuron state and commands the shaper stage. An hysteresis behavior is obtained by setting the feedback transistors Q_7 and Q_8 such that $W_{Q7}/W_{Q6} = W_{Q8}/W_{Q9} > 1$ for the same transistor length.

Table 3: Comparison between state-of-the-art ONN Integrated Circuits

	Jackson et. al. [5]	Ahmed et. al. [11]	Bashar et. al. [19]	Graber et. al. [20]	This work
Technology	28nm	65nm	65nm	28nm	65nm
Neurons	100	560	30	400	16
Connectivity	all-to-all	hexagonal	all-to-all	King's graph	all-to-all
Power	303 mW	23 mW	1.76 mW	182 mW	160 μ W
Frequency	1 GHz	118 MHz	45 kHz	200 MHz	1 MHz
Energy/osc	0.30 pJ	0.35 pJ	1.3 nJ	2.3 pJ	10 pJ
Chip area	3.24 mm ²	1.44 mm ²	-	2.2 mm ²	3.9 mm ²

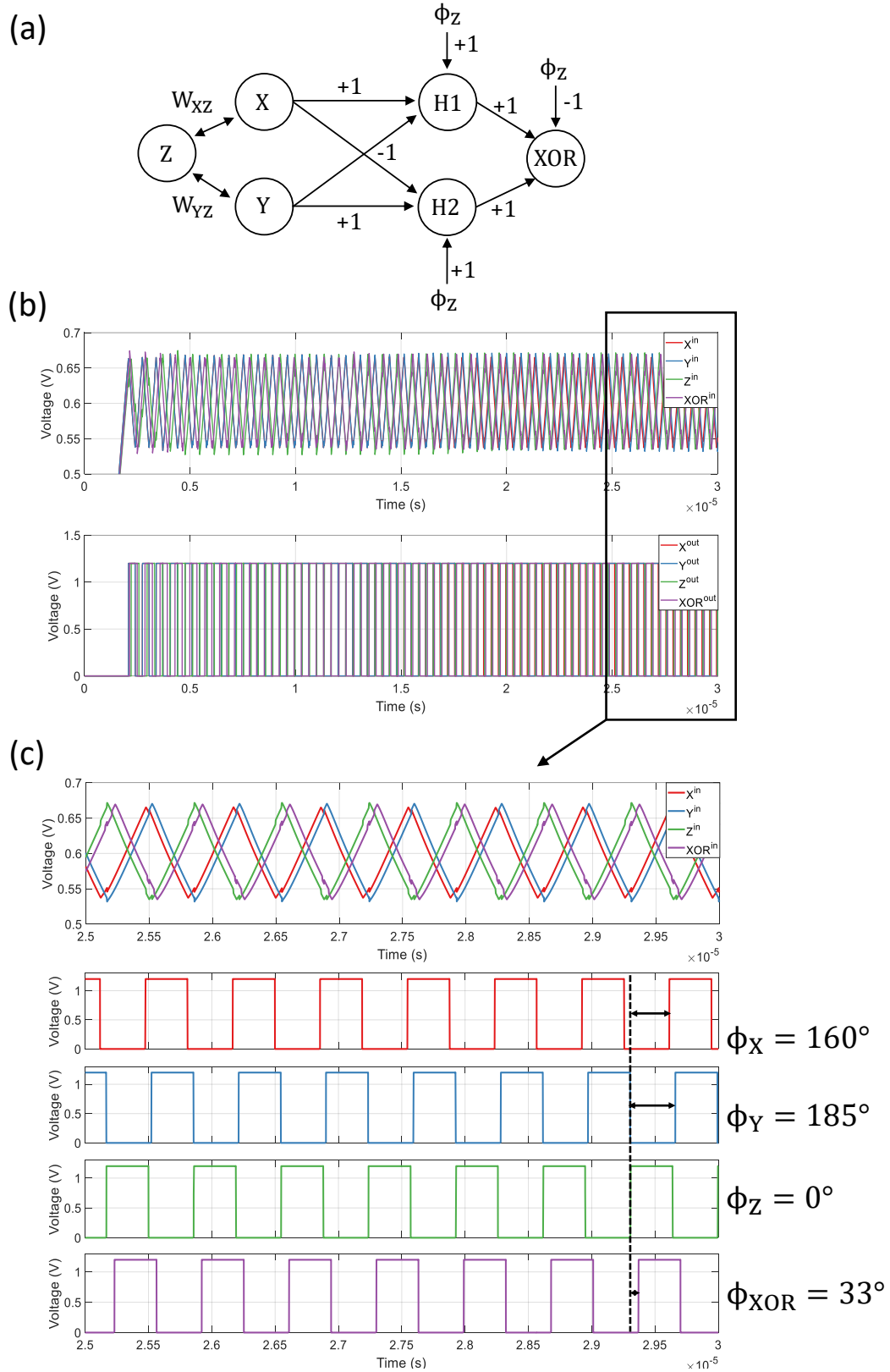


Figure 10: a) XOR(X,Y) circuit using SKONN and feed-forward synapses. Neuron Z is the reference oscillator and can be thought of as the neurons' bias, similar to perceptrons. The weights W_{XZ} and W_{YZ} are the inputs and set the initial phases ϕ_X and ϕ_Y . b) Example of dynamics when $W_{XZ} = W_{YZ} = -1$ which set $\phi_X = \phi_Y = 180^\circ$ and corresponds to the boolean case where $X=Y=1$. c) Zoom on the steady-state solution.

Table 4: Solving XOR(X,Y) with SKONN

W_{XZ}	W_{YZ}	ϕ_X	ϕ_Y	ϕ_{XOR}
+1	+1	6°	341°	33°
+1	-1	340°	185°	185°
-1	+1	185°	340°	185°
-1	-1	160°	185°	33°

oscillators toward the desired value which is challenging to obtain with recurrent synapses. Instead, teaching oscillators could drive the output oscillators using feed-forward connections without being impacted during the learning phase.

To demonstrate the SKONN feed-forward ability, we run ASIC transient simulations of a simple 2-input XOR operation. Inspired by the Parametron built by Goto in the 1950s [3], we use a 3-input SKONN neuron as a majority gate

$$\phi_M = (\phi_X \cdot \phi_Y) + (\phi_X \cdot \phi_Z) + (\phi_Y \cdot \phi_Z) \quad (18)$$

Where $\phi_X, \phi_Y, \phi_Z \in \{0; 180\}$ are the input binary phases thought as Boolean variables; i.e. ϕ_M is true when $\phi_M=180^\circ$. Interestingly, SKONN's odd-degree property (Proposition 2.1) ensures that ϕ_M is binary when its inputs are also binary.

The XOR(X,Y) circuit is implemented by writing the XOR boolean expression $\phi_{XOR} = (\phi_X \cdot \overline{\phi_Y}) + (\phi_Y \cdot \overline{\phi_X})$. Considering ϕ_Z as the reference oscillator, AND and OR gates are obtained when feeding ϕ_Z or $\overline{\phi_Z}$ to the majority gates, respectively. Fig.10a shows the obtained network with two hidden neurons (H1,H2), one neuron acting as a bias unit (Z), and one output neuron. The two input neurons X and Y are recurrently connected to the reference oscillator Z to set the input phase ϕ_X and ϕ_Y . When the weight W_{XZ} is -1 or +1, it sets $\phi_X \approx 0^\circ$ or $\phi_X \approx 180^\circ$, respectively, and the same rule applies for ϕ_Y and W_{YZ} . All the oscillators are arbitrarily turned on at the same time before the input phases ϕ_X and ϕ_Y settle to the desired inputs. Then, the network further relaxes to a stable phase state after a few oscillations and we read the output phase ϕ_{XOR} . Fig.10b and c show the simulation results in the case $\phi_{XOR}(180^\circ, 180^\circ) = 0^\circ$. Table 4 summarizes the results for the 4 possible inputs W_{XZ} and W_{YZ} . By assigning the bit 0 when $270^\circ \leq \phi_i \leq 90^\circ$ and 1 otherwise, it can be seen that the proposed network computes XOR(X,Y) in a feed-forward manner.

3.4 SKONN scaling and benchmarking

3.4.1 Weighted Max-cut of random graphs

To assess how SKONN's computational performances scale, we run large-scale simulations of random Weighted Max-cut problems for N=8, 16, 32, 64, 128, 256, 512, and 1024 nodes. For each graph density $d=0.25, 0.5,$ and $0.75,$ 10 random graphs $G(N, d)$ are generated such that the total number of edges $m = d N(N - 1)/2$. The graph edges are randomly weighted with positive values from 0 to 15 that correspond to the ASIC synaptic range. We use the ASIC parameters and solve SKONN's dynamics (7) with MATLAB using the built-in ODE solver ode15s. For each graph instance, we run 10 trials with random phase initialization, for a total of 100 trials per graph size and density. As a ground truth, we consider the best solution Cut_{GW} provided by the Goemans-Williamson algorithm, out of 100 random projections defining the cut [36] and computed with the CVX solver on MATLAB [47]. The distance between the SDP cut Cut_{SDP} and Cut_{GW} is represented in Fig.11a. As $Cut_{SDP} \geq \text{Max-cut}$, the ratio Cut_{GW}/Cut_{SDP} gives a lower bound on the chosen GW cut. For all the trials, the results are compared with Kuramoto dynamics with the same parameters and initializations.

Fig.11b shows SKONN's and Kuramoto's phase distributions for each ONN size. Here again, it appears that SKONN phases tend to be clustered near 0° and 180° whereas Kuramoto phases seem more uniformly distributed. Fig.11c present the obtained cuts when considering the first oscillator as the reference, and normalized by Cut_{GW} . We first notice that the results are quite homogeneous with respect to the graph densities. Secondly, it appears that SKONN produces high-quality cuts as $Cut/Cut_{GW} \approx 1$ for all ONN sizes. In contrast, Kuramoto-ONNs have a lower accuracy for sizes between N=16 and N=256. Interestingly, the settling time (time to reach a steady phase state) seems to grow according to a logarithmic law with the ONN size. This result refines some previous scaling observations mentioning a quasi-constant settling time [16, 8]. It also confirms the high ONN parallelism and ability to compute in a few tens of cycles, even for large graphs.

Similarly to the CirCut algorithm [37] (rank-2 relaxation approach), we also investigate the Kuramoto accuracy when changing the reference oscillator and name it the "Kuramoto-CirCut" scheme. Fig.11d presents the case where the best Kuramoto cut is chosen out of N possible cuts, whereas the SKONN reference oscillator remains the first one. It can be seen that SKONN provides the same quality cut as GW and Kuramoto-CirCut. However, compared to GW and Kuramoto-CirCut, SKONN's cut is solely obtained by reading out the phases with respect to a single oscillator and does not need N different cut evaluations that linearly increase the time to solution.

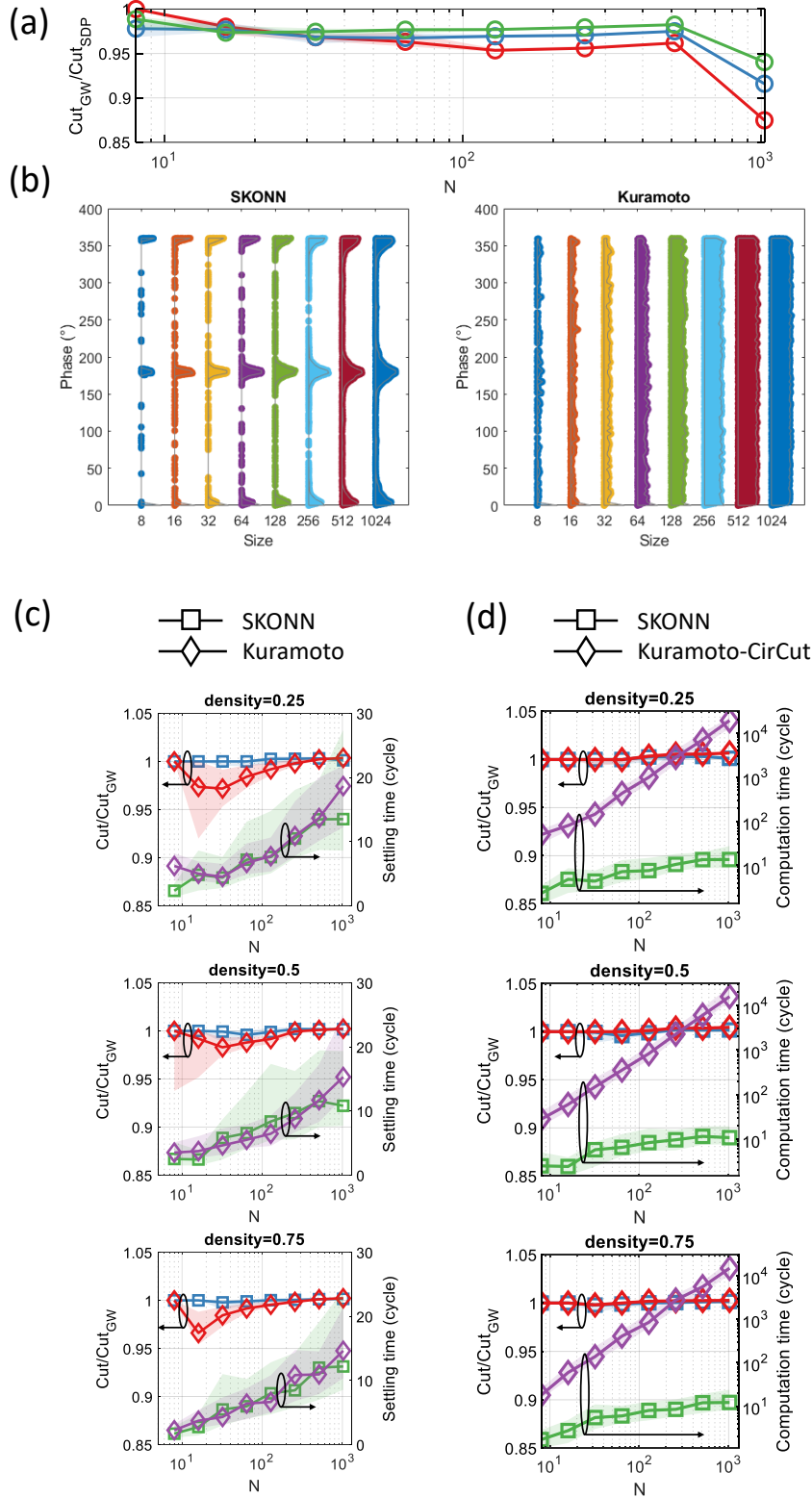


Figure 11: a) Ratio between Cut_{GW} and Cut_{SDP} that gives a lower bound on Cut_{GW} as $Cut_{SDP} \geq \text{Max-cut}$. b) Phase distribution at steady state for SKONN (left) and Kuramoto (right) for various ONN sizes. c) Cuts obtained by SKONN and Kuramoto when the first oscillator is the phase reference and for various graph densities. d) Cut obtained when SKONN's reference is the first oscillator, compared to the case where the Kuramoto reference is changed N times, similarly to the CirCut algorithm [37].

Table 5: Comparison Between CirCut, Kuramoto, and SKONN solvers for G-SET Max-cut instances. The bold values indicate the best cut obtained among the four approaches. The number in parenthesis is the cut normalized by the best-known cut found in [48].

Graph				Value					Settling time (cycles)	
Name	(V , E)	Weights	Type	GW	Kuramoto-CirCut	Kuramoto	SKONN	Best-known [48]	Kuramoto	SKONN
G11	(800, 1600)	-1,+1	toroidal	530 (0.940)	514 (0.911)	502 (0.890)	540 (0.957)	564	480	368
G12	(800, 1600)	-1,+1	toroidal	532 (0.957)	510 (0.917)	496 (0.892)	528 (0.950)	556	216	272
G13	(800, 1600)	-1,+1	toroidal	554 (0.952)	538 (0.924)	524 (0.900)	544 (0.935)	582	368	224
G14	(800, 4694)	+1	planar	2978 (0.972)	3005 (0.981)	2974 (0.970)	3020 (0.986)	3064	416	496
G15	(800, 4661)	+1	planar	2963 (0.971)	2992 (0.981)	2970 (0.974)	2979 (0.977)	3050	704	240
G20	(800, 4672)	-1,+1	planar	849 (0.902)	871 (0.926)	818 (0.869)	858 (0.912)	941	504	208
G21	(800, 4667)	-1,+1	planar	849 (0.911)	868 (0.932)	839 (0.901)	852 (0.915)	931	184	104
G22	(2000, 19990)	+1	random	12936 (0.968)	13095 (0.980)	13026 (0.975)	12988 (0.972)	13359	280	104
G23	(2000, 19990)	+1	random	12946 (0.970)	13106 (0.982)	13078 (0.980)	12950 (0.970)	13344	864	216
G24	(2000, 19990)	+1	random	12966 (0.972)	13135 (0.985)	13050 (0.978)	12997 (0.974)	13337	928	160
G30	(2000, 19990)	-1,+1	random	3014 (0.883)	3200 (0.938)	3175 (0.930)	3095 (0.907)	3413	376	192
G31	(2000, 19990)	-1,+1	random	2885 (0.872)	3089 (0.933)	3063 (0.925)	3015 (0.911)	3310	1424	456
G32	(2000, 4000)	-1,+1	toroidal	1290 (0.915)	1284 (0.911)	1280 (0.908)	1332 (0.944)	1410	616	520
G33	(2000, 4000)	-1,+1	toroidal	1266 (0.916)	1254 (0.907)	1244 (0.900)	1294 (0.936)	1382	424	248
G34	(2000, 4000)	-1,+1	toroidal	1274 (0.920)	1258 (0.909)	1224 (0.884)	1306 (0.943)	1384	704	456
G50	(3000, 6000)	-1,+1	toroidal	5880 (1.00)	5784 (0.983)	5764 (0.980)	5818 (0.989)	5880	544	1968
G56	(5000, 12498)	-1,+1	random	3634 (0.904)	3700 (0.921)	3622 (0.901)	3733 (0.929)	4017	712	296
G57	(5000, 10000)	-1,+1	toroidal	3320 (0.950)	3138 (0.898)	3054 (0.874)	3270 (0.936)	3494	792	576
G60	(7000, 17148)	+1	random	13610 (0.959)	13730 (0.968)	13669 (0.963)	13717 (0.967)	14188	824	384
G61	(7000, 17148)	-1,+1	random	5252 (0.906)	5322 (0.918)	5257 (0.907)	5327 (0.919)	5796	1648	312
G62	(7000, 14000)	-1,+1	toroidal	4612 (0.947)	4394 (0.902)	4358 (0.895)	4642 (0.953)	4870	520	1328
G64	(7000, 41459)	-1,+1	planar	7624 (0.871)	8046 (0.919)	7946 (0.908)	8135 (0.930)	8751	800	352
Average				0.934	0.938	0.923	0.946	1	623	431

3.4.2 G-set benchmark

The previous study concerned random graphs. Here, we benchmark SKONN for solving Max-cut using the G-set benchmark that includes various graph topologies [48]. Table 5 shows the cuts obtained for a single trial with SKONN and Kuramoto using the same random phase initialization, and considering the first oscillator as the phase reference. The cuts are compared against the state-of-the-art GW [36] and the Kuramoto-CirCut scheme [37]. GW’s cut is the best cut obtained out of 100 random projections and computed with the CVX solver on MATLAB [47]. For graphs with $N > 3000$, GW values are taken from another state-of-the-art SDP solver [49] due to memory constraints. The Kuramoto-CirCut values correspond to the best cut extracted from the Kuramoto dynamics, out of N possible reference oscillators.

With a single run, Kuramoto-CirCut and SKONN solvers produce, on average, better results than the GW algorithm which picks up the best spin configuration out of 100 random projections. The average SKONN cut value is 94.6% of the best-known cuts [48] and the highest among the four methods. The accuracy obtained by simulating SKONN motivates its real hardware implementation as the time-to-solution could be drastically reduced compared to a CPU. For instance, solving the smallest graph G11 requires 12 s of GW runtime on a laptop (i7 Intel core @ 1.6 GHz and 32 GB of RAM). In contrast, SKONN’s settling time does not vary much with the ONN size and could enable a large-scale cut computation in less than 431 cycles on average. With oscillators running at 1 MHz, the runtime per trial would only be 431 μ s which is $2.8 \cdot 10^4$ x faster than GW’s execution. However, reaching excellent cuts such as 99.9% of the best-known cut requires more trials and annealing the ONN to escape local minima. For more results using SHIL and various annealing schemes, please refer to [8].

4 Discussion

SKONN mixed-signal architecture facilitates scaling up the ONN size thanks to the separation between analog computation and digital propagation. While the neurons exchange information in the digital domain, SKONN architecture ensures that the sensitive analog computation remains within modules and can be shielded from the outside. However, it remains some design challenges that are currently being investigated:

1. Any delay added to the digital propagation is equivalent to a synaptic phase shift. This must be considered for a high-frequency operation when buffers’ delays become non-negligible and can be an issue for advanced technologies.

2. Large synaptic values can induce large voltage jumps at the analog input that can decrease the frequency for recurrent synapses, as highlighted in Fig.6d. Without compensation, this strong coupling scenario could lead to multiple oscillation frequencies and prevent global phase-locking.

5 Conclusion

This article introduced SKONN, a novel mixed-signal ONN architecture that enables large-scale analog computations in phase domain. We presented how the association of simple circuitry can enable robust analog phase computation; while propagating the information in the digital domain to facilitate the implementation of large networks. We first reported experiments on a 9-neuron SKONN on PCB that finds the maximum cut of weighted graphs with high accuracy. Then, we presented the design of a CMOS 16-neuron integrated circuit (IC), highlighting SKONN programmability, modularity, and benchmarking with state-of-the-art ONN ICs. Furthermore, our design choice led to interesting phase dynamics that are a *saturated* version of the Kuramoto model and have unique properties. Such as, we found that such dynamics tend to binarize phases and are very efficient to solve NP-hard problems based on binary variables like Max-Cut. It appeared that SKONN's accuracy on random graphs is as good as the state-of-the-art Goemans-Williamson (GW) and CirCut algorithms, and even higher when benchmarked with graphs with up to 7000 nodes from the G-set. Our study revealed that SKONN's computation time grows logarithmically with the network size which is promising for solving large-scale problems. For example, SKONN neurons oscillating at 1 MHz would provide a graph cut four orders of magnitude faster than the GW algorithm run on a CPU.

Acknowledgments

We thank Laurent Deknyff from LIRMM, CNRS, for his circuit design expertise and for fabricating the PCB proof-of-concept. We also thank Jeremie Salles and Fathi Ben Ali from LIRMM, CNRS, for their support during the IC design.

Declarations

This work was supported by the European Union's Horizon 2020 research and innovation program, EU H2020 NEURONN (www.neuronn.eu) project under Grant 871501.

References

- [1] Christiaan Huygens. *Oeuvres complètes de Christiaan Huygens. Publiées par la Société hollandaise des sciences*, volume 1. La Haye, M. Nijhoff, 1888-1950.
- [2] John von Neumann. Non-linear capacitance or inductance switching, amplifying and memory devices. 1954.
- [3] Eiichi Goto. The parametron, a digital computing element which utilizes parametric oscillation. *Proceedings of the IRE*, 47(8):1304–1316, 1959.
- [4] S. Takahashi. A brief history of the japanese computer industry before 1985. *IEEE Annals of the History of Computing*, 18(01):76, jan 1996.
- [5] Thomas Jackson, Samuel Pagliarini, and Lawrence Pileggi. An oscillatory neural network with programmable resistive synapses in 28 nm cmos. In *2018 IEEE International Conference on Rebooting Computing (ICRC)*, pages 1–7, 2018.
- [6] Elisabetta Corti, Joaquin Antonio Cornejo Jimenez, Kham M. Niang, John Robertson, Kirsten E. Moselund, Bernd Gotsmann, Adrian M. Ionescu, and Siegfried Karg. Coupled vo2 oscillators circuit as analog first layer filter in convolutional neural networks. *Frontiers in Neuroscience*, 15, 2021.
- [7] Corentin Delacour, Stefania Carapezzi, Madeleine Abernot, Gabriele Boschetto, Nadine Azemard, Jeremie Salles, Thierry Gil, and Aida Todri-Sanial. Oscillatory neural networks for edge ai computing. In *2021 IEEE Computer Society Annual Symposium on VLSI (ISVLSI)*, pages 326–331, 2021.
- [8] Tianshi Wang, Leon Wu, Parth Nobel, and Jaijeet Roychowdhury. Solving combinatorial optimisation problems using oscillator based ising machines. *Natural Computing*, 20(2):287–306, Jun 2021.
- [9] S. Dutta, A. Khanna, A. S. Assoa, H. Paik, D. G. Schlom, Z. Toroczkai, A. Raychowdhury, and S. Datta. An ising hamiltonian solver based on coupled stochastic phase-transition nano-oscillators. *Nature Electronics*, 4(7):502–512, Jul 2021.

- [10] Antik Mallick, Mohammad Khairul Bashar, Daniel S. Truesdell, Benton H. Calhoun, Siddharth Joshi, and Nikhil Shukla. Using synchronized oscillators to compute the maximum independent set. *Nature Communications*, 11(1):4689, Sep 2020.
- [11] Ibrahim Ahmed, Po-Wei Chiu, William Moy, and Chris H. Kim. A probabilistic compute fabric based on coupled ring oscillators for solving combinatorial optimization problems. *IEEE Journal of Solid-State Circuits*, 56(9):2870–2880, 2021.
- [12] J J Hopfield. Neural networks and physical systems with emergent collective computational abilities. *Proceedings of the National Academy of Sciences*, 79(8):2554–2558, 1982.
- [13] Eugene Izhikevich and Yoshiki Kuramoto. Weakly coupled oscillators. *Encyclopedia of Mathematical Physics*, 12 2006.
- [14] Toshio Aoyagi. Network of neural oscillators for retrieving phase information. *Physical review letters*, 74:4075–4078, 06 1995.
- [15] F.C. Hoppensteadt and E.M. Izhikevich. Pattern recognition via synchronization in phase-locked loop neural networks. *IEEE Transactions on Neural Networks*, 11(3):734–738, 2000.
- [16] Corentin Delacour, Stefania Carapezzi, Madeleine Abernot, and Aida Todri-Sanial. Energy-performance assessment of oscillatory neural networks based on vo_2 devices for future edge ai computing. *IEEE Transactions on Neural Networks and Learning Systems*, pages 1–14, 2023.
- [17] Tianshi Wang, Leon Wu, and Jaijeet Roychowdhury. New computational results and hardware prototypes for oscillator-based ising machines. In *Proceedings of the 56th Annual Design Automation Conference 2019, DAC '19*, New York, NY, USA, 2019. Association for Computing Machinery.
- [18] Jeffrey Chou, Suraj Bramhavar, Siddhartha Ghosh, and William Herzog. Analog coupled oscillator based weighted ising machine. *Scientific Reports*, 9(1):14786, Oct 2019.
- [19] Mohammad Khairul Bashar, Antik Mallick, and Nikhil Shukla. Experimental investigation of the dynamics of coupled oscillators as ising machines. *IEEE Access*, 9:148184–148190, 2021.
- [20] Markus Graber and Klaus Hofmann. A versatile adjustable 400 node cmos oscillator based ising machine to investigate and optimize the internal computing principle. In *2022 IEEE 35th International System-on-Chip Conference (SOCC)*, pages 1–6, 2022.
- [21] Gyorgy Csaba and Wolfgang Porod. Coupled oscillators for computing: A review and perspective. *Applied Physics Reviews*, 7(1):011302, 2020.
- [22] Jacob Torrejon, Mathieu Riou, Flavio Abreu Araujo, Sumito Tsunegi, Guru Khalsa, Damien Querlioz, Paolo Bortolotti, Vincent Cros, Kay Yakushiji, Akio Fukushima, Hitoshi Kubota, Shinji Yuasa, Mark D. Stiles, and Julie Grollier. Neuromorphic computing with nanoscale spintronic oscillators. *Nature*, 547(7664):428–431, Jul 2017.
- [23] J. Grollier, D. Querlioz, K. Y. Camsari, K. Everschor-Sitte, S. Fukami, and M. D. Stiles. Neuromorphic spintronics. *Nature Electronics*, 3(7):360–370, Jul 2020.
- [24] Paolo Maffezzoni, Bichoy Bahr, Zheng Zhang, and Luca Daniel. Analysis and design of boolean associative memories made of resonant oscillator arrays. *IEEE Transactions on Circuits and Systems I: Regular Papers*, 63(11):1964–1973, 2016.
- [25] F.C. Hoppensteadt and E.M. Izhikevich. Synchronization of mems resonators and mechanical neurocomputing. *IEEE Transactions on Circuits and Systems I: Fundamental Theory and Applications*, 48(2):133–138, 2001.
- [26] Nikhil Shukla, Abhinav Parihar, Eugene Freeman, Hanjong Paik, Greg Stone, Vijaykrishnan Narayanan, Haidan Wen, Zhonghou Cai, Venkatraman Gopalan, Roman Engel-Herbert, Darrell G. Schlom, Arijit Raychowdhury, and Suman Datta. Synchronized charge oscillations in correlated electron systems. *Scientific Reports*, 4(1):4964, May 2014.
- [27] Stefania Carapezzi, Gabriele Boschetto, Corentin Delacour, Elisabetta Corti, Andrew Plews, Ahmed Nejm, Siegfried Karg, and Aida Todri-Sanial. Advanced design methods from materials and devices to circuits for brain-inspired oscillatory neural networks for edge computing. *IEEE Journal on Emerging and Selected Topics in Circuits and Systems*, 11(4):586–596, 2021.
- [28] Thomas C. Jackson, Abhishek A. Sharma, James A. Bain, Jeffrey A. Weldon, and Lawrence Pileggi. Oscillatory neural networks based on tmo nano-oscillators and multi-level rram cells. *IEEE Journal on Emerging and Selected Topics in Circuits and Systems*, 5(2):230–241, 2015.
- [29] S. Dutta, A. Khanna, W. Chakraborty, J. Gomez, S. Joshi, and S. Datta. Spoken vowel classification using synchronization of phase transition nano-oscillators. In *2019 Symposium on VLSI Circuits*, pages T128–T129, 2019.

- [30] Dmitri Nikonov, Peter Kurahashi, James Ayers, Hai Li, Telesphor Kamgaing, Georgios Dogiamis, Hyung-Jin Lee, Yongping Fan, and I. Young. Convolution inference via synchronization of a coupled cmos oscillator array. *IEEE Journal on Exploratory Solid-State Computational Devices and Circuits*, PP:1–1, 12 2020.
- [31] Arkosnato Neogy and Jaijeet Roychowdhury. Analysis and design of sub-harmonically injection locked oscillators. In *2012 Design, Automation Test in Europe Conference Exhibition (DATE)*, pages 1209–1214, 2012.
- [32] Prateek Bhansali and Jaijeet Roychowdhury. Gen-adler: The generalized adler’s equation for injection locking analysis in oscillators. In *2009 Asia and South Pacific Design Automation Conference*, pages 522–527, 2009.
- [33] Aida Todri-Sanial, Stefania Carapezzi, Corentin Delacour, Madeleine Abernot, Thierry Gil, Elisabetta Corti, Siegfried F. Karg, Juan Núñez, Manuel Jiménez, María J. Avedillo, and Bernabé Linares-Barranco. How frequency injection locking can train oscillatory neural networks to compute in phase. *IEEE Transactions on Neural Networks and Learning Systems*, 33(5):1996–2009, 2022.
- [34] Corentin Delacour and Aida Todri-Sanial. Mapping hebbian learning rules to coupling resistances for oscillatory neural networks. *Frontiers in Neuroscience*, 15, 2021.
- [35] Frank C. Hoppensteadt and Eugene M. Izhikevich. *Weakly Connected Oscillators*, pages 247–293. Springer New York, New York, NY, 1997.
- [36] Michel X. Goemans and David P. Williamson. Improved approximation algorithms for maximum cut and satisfiability problems using semidefinite programming. *J. ACM*, 42:1115–1145, 1995.
- [37] Samuel Burer, Renato Monteiro, and Yin Zhang. Rank-two relaxation heuristics for max-cut and other binary quadratic programs. *SIAM Journal on Optimization*, 12, 07 2001.
- [38] Toshimori Honjo, Tomohiro Sonobe, Kensuke Inaba, Takahiro Inagaki, Takuya Ikuta, Yasuhiro Yamada, Takushi Kazama, Koji Enbutsu, Takeshi Umeki, Ryoichi Kasahara, Ken ichi Kawarabayashi, and Hiroki Takesue. 100,000-spin coherent ising machine. *Science Advances*, 7(40):eabh0952, 2021.
- [39] Ryan Hamerly, Takahiro Inagaki, Peter L. McMahon, Davide Venturelli, Alireza Marandi, Tatsuhiro Onodera, Edwin Ng, Carsten Langrock, Kensuke Inaba, Toshimori Honjo, Koji Enbutsu, Takeshi Umeki, Ryoichi Kasahara, Shoko Utsunomiya, Satoshi Kako, Ken ichi Kawarabayashi, Robert L. Byer, Martin M. Fejer, Hideo Mabuchi, Dirk Englund, Eleanor Rieffel, Hiroki Takesue, and Yoshihisa Yamamoto. Experimental investigation of performance differences between coherent ising machines and a quantum annealer. *Science Advances*, 5(5):eaau0823, 2019.
- [40] Fuxi Cai, Suhas Kumar, Thomas Van Vaerenbergh, Xia Sheng, Rui Liu, Can Li, Zhan Liu, Martin Foltin, Shimeng Yu, Qiangfei Xia, J. Joshua Yang, Raymond Beausoleil, Wei D. Lu, and John Paul Strachan. Power-efficient combinatorial optimization using intrinsic noise in memristor hopfield neural networks. *Nature Electronics*, 3(7):409–418, Jul 2020.
- [41] Ernst Ising. Beitrag zur theorie des ferromagnetismus. *Zeitschrift für Physik*, 31(1):253–258, Feb 1925.
- [42] Andrew Lucas. Ising formulations of many np problems. *Frontiers in Physics*, 2, 2014.
- [43] Mikhail Erementchouk, Aditya Shukla, and Pinaki Mazumder. On computational capabilities of ising machines based on nonlinear oscillators. *Physica D: Nonlinear Phenomena*, 437:133334, 2022.
- [44] Paul Erdős, Alfréd Rényi, et al. On the evolution of random graphs. *Publ. Math. Inst. Hung. Acad. Sci*, 5(1):17–60, 1960.
- [45] Benjamin Scellier and Yoshua Bengio. Equilibrium propagation: Bridging the gap between energy-based models and backpropagation. *Frontiers in Computational Neuroscience*, 11, 2017.
- [46] Gianluca Zoppo, Francesco Marrone, Michele Bonnin, and Fernando Corinto. Equilibrium propagation and (memristor-based) oscillatory neural networks. In *2022 IEEE International Symposium on Circuits and Systems (ISCAS)*, pages 639–643, 2022.
- [47] Michael Grant and Stephen Boyd. CVX: Matlab software for disciplined convex programming, version 2.1. <http://cvxr.com/cvx>, March 2014.
- [48] Duarte Martí. G-set data for max-cut. <https://grafo.etsii.urjc.es/opticom/maxcut.html>, 2009.
- [49] Changhui Choi and Yinyu Ye. Solving sparse semidefinite programs using the dual scaling algorithm with an iterative solver. *Manuscript, Department of Management Sciences, University of Iowa, Iowa City, IA, 52242*, 2000.
- [50] Paolo Maffezzoni, Luca Daniel, Nikhil Shukla, Suman Datta, and Arijit Raychowdhury. Modeling and simulation of vanadium dioxide relaxation oscillators. *IEEE Transactions on Circuits and Systems I: Regular Papers*, 62(9):2207–2215, 2015.

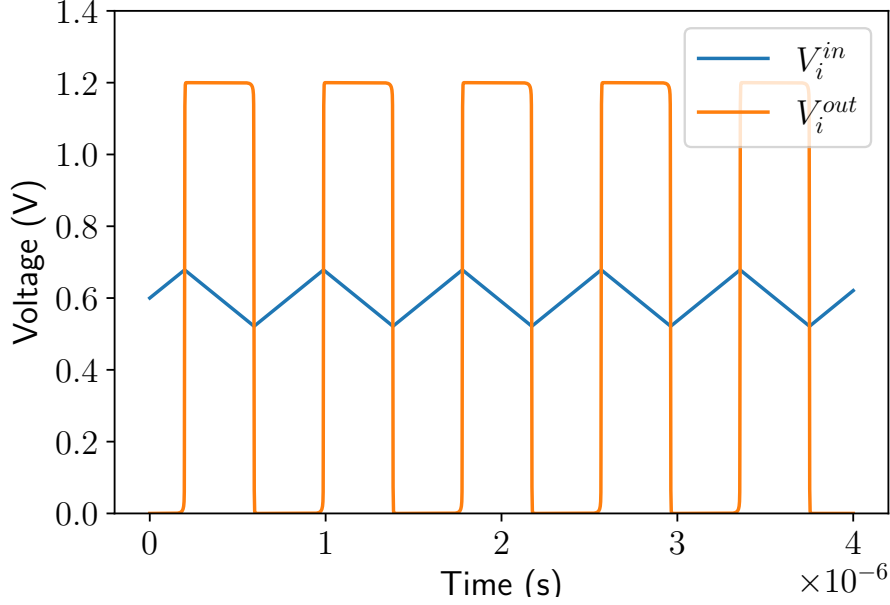


Figure 12: Voltage dynamics of a single neuron obtained by solving numerically (19). In this example, $C_L=500\text{fF}$, $I_{bias}=200\text{nA}$, $V_L=0.5\text{V}$, $V_H=0.7\text{V}$, $V_{DD}=1.2\text{V}$, $\gamma=100$ and $\tau_H=1\text{ns}$.

A SKONN voltage and current dynamics

A.1 Neuron voltage dynamics

By denoting I_{ij} the input synaptic currents, the voltage dynamics of neuron i can be modeled as follows:

$$\begin{cases} C_L \frac{dV_i^{in}}{dt} = I_{bias} \text{sign}\left(V_{DD}/2 - V_i^{out}\right) + \sum_j I_{ij} \\ \tau_H \frac{dV_i^{out}}{dt} = V_{DD} f_H\left(V_i^{in}, V_i^{out}, V_L, V_H\right) - V_i^{out} \end{cases} \quad (19)$$

Where C_L is the input capacitance, I_{bias} the current that charges and discharges C_L , V_{DD} is the amplitude of V_i^{out} , V_L and V_H are the lower and upper thresholds of the hysteresis block, and τ_H is the time constant linked to the output load of the hysteresis block. The term f_H expresses the output switching with hysteresis behavior. As in [50], one can model the hysteresis behavior using a tanh function with slope γ :

$$f_H = 0.5 \left(1 + \tanh\left(\gamma \left(V_i^{in} - V_H - \frac{V_L - V_H}{V_{DD}} V_i^{out} \right) \right) \right) \quad (20)$$

When $f_H=0$, $V_i^{out}=0$ and C_L charges. When $f_H = 1$, $V_i^{out}=V_{DD}$ and C_L discharges. The two switching occur when $V_i^{in}=V_L$ and $V_i^{in}=V_H$, respectively. Fig.12 shows an example of numerical solution for the equations (19).

A.2 Synaptic currents

In SKONN, the digital output voltage V_j^{out} goes through the synaptic capacitance C_{ij} that creates current spikes holding the phase information ϕ_j . The synaptic spike train can be expressed as follows:

$$I_{ij} = C_{ij} \left(\frac{dV_j^{out}}{dt} - \frac{dV_i^{in}}{dt} \right) \quad (21)$$

A.3 Voltage dynamics of coupled neurons

By injecting the synaptic current expression in equation (19), we obtain:

SKONN PPV

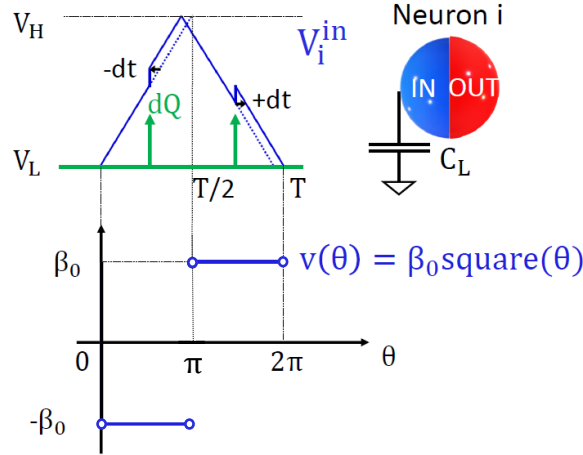


Figure 13: SKONN Phase Perturbation Vector (PPV). The injection of a charge dQ induces a time shift $\pm dt$, which in turn creates a phase shift $d\phi = 2\pi dt/T$. The phase shift sign changes when there is a change in V_i^{in} 's slope.

$$\begin{cases} C_{eq} \frac{dV_i^{in}}{dt} = I_{bias} \text{sign}(V_i^{out} - V_{DD}/2) + \sum_j C_{ij} \frac{dV_j^{out}}{dt} \\ \tau_H \frac{dV_i^{out}}{dt} = V_{DD} f_H(V_i^{in}, V_i^{out}, V_L, V_H) - V_i^{out} \end{cases} \quad (22)$$

With C_{eq} the equivalent capacitance:

$$C_{eq} = C_L + \sum_j C_{ij} \quad (23)$$

(23) indicates that the synaptic capacitances are added to the oscillator load and slow down the charge and discharge of the input node. Large synaptic capacitances could potentially induce heterogeneous frequencies within SKONN and still needs to be explored.

B SKONN Phase Perturbation Vector

The PPV is a T -periodic function $\vec{v}(t)$ that quantifies the phase shift of an oscillator subject to a perturbation occurring at time t [32]. One way of computing $\vec{v}(t)$ is to inject a pulsed perturbation to the oscillator at time t , measure the induced phase shift and normalize by the perturbation's strength [9]. In SKONN, the synaptic current I_{ij} perturbs the triangular oscillation V_i^{in} and the scalar PPV $v(t)$ can be derived by computing the phase shift $d\phi$ when injecting current pulses $I(t') = dQ\delta(t' - t)$ with $t \in [0; T]$. From Fig.13, we distinguish three cases:

1. $0 < t < T/2$: the perturbed oscillation is shifted toward the left by the same amount of time $-dt$.
2. $T/2 < t < T$: the perturbed oscillation is shifted toward the right by the same amount of time $+dt$.
3. $t \in \{0; T/2\}$: the time shift is undefined as V_i^{in} 's slope is undefined (not derivable).

Injecting dQ to C_L induces a voltage jump $dV = dQ/C_L$. This results in a time delay $-dt$ and $+dt$ when C_L charges and discharges, respectively, with $|dt| = C_L dV / I_{bias}$. The amount of phase shift can then be expressed as $d\phi = 2\pi dt/T$. The oscillation period T is expressed by $T = 2C_L \Delta V / I_{bias}$, with $\Delta V = V_H - V_L$. Finally, merging the equations leads to

$$\frac{d\phi}{dQ} = \pm \frac{\pi}{C_L \Delta V} = \pm \beta_0 \quad (24)$$

Which is the phase shift caused by the injection of 1 coulomb. The phase shift sign depends on whether the charge is injected during the charge or discharge of the triangular waveform. Considering the three previous cases and changing the time variable t to phase θ , we express SKONN's PPV as follows:

$$v(\theta) = \beta_0 \text{square}(\theta) \quad (25)$$

Where:

$$\text{square}(\theta) = \begin{cases} -1, & \text{if } 0 < \theta < \pi \\ +1, & \text{if } \pi < \theta < 2\pi \end{cases} \quad (26)$$

C SKONN phase dynamics

C.1 Two coupled oscillators

The phase dynamics of a single oscillator of frequency $\omega_0 = 2\pi/T$ are:

$$\frac{d}{dt}\phi(t) = \omega_0 \quad (27)$$

When the oscillator receives a pre-synaptic signal $\vec{b}(t)$, it undergoes a time shift $\alpha(t)$ associated with the perturbation $\vec{b}(t)$. If the variation of the oscillating amplitude remains small [32], $\alpha(t)$ dynamics can be expressed as follows:

$$\frac{d}{dt}\alpha(t) = \vec{v}(t + \alpha(t)) \cdot \vec{b}(t) \quad (28)$$

Where $\vec{v}(t)$ is the T-periodic Phase Perturbation Vector (PPV) associated with the oscillator; and describes the phase sensitivity of the oscillator under injections at different nodes. In our case, we consider scalars $b(t)$ and $v(t)$ as the pre-synaptic signal $b(t)$ is injected to a unique input node. As $b(t)$ also oscillates at frequency ω_0 and with phase $\phi_b(t) = \omega_0 t$, we introduce $\Delta\phi(t) = \phi(t) - \phi_b(t) = \omega_0 \alpha(t)$ that expresses the phase difference between post and presynaptic signals. The latter can be considered as the reference as it is driving the oscillator. To simplify equations, we define the 2π -periodic PPV and perturbation as $v^{2\pi}(\omega_0 t) = v(t)$ and $b^{2\pi}(\omega_0 t) = b(t)$, respectively. The phase dynamics become:

$$\frac{d}{dt}\Delta\phi = \omega_0 v^{2\pi}(\phi_b + \Delta\phi) b^{2\pi}(\phi_b) \quad (29)$$

We assume that under weak coupling, the phase difference $\Delta\phi$ evolves slowly compared to the presynaptic phase ϕ_b and it is common practice to average out $\Delta\phi$ over one period:

$$\begin{aligned} \frac{1}{2\pi} \int_{-\pi}^{\pi} \frac{d}{dt}\Delta\phi d\phi_b &\approx \frac{d}{dt}\Delta\phi \\ &= \frac{1}{T} \int_{-\pi}^{\pi} v^{2\pi}(\phi_b + \Delta\phi) b^{2\pi}(\phi_b) d\phi_b \end{aligned} \quad (30)$$

We saw previously that a pre-synaptic signal consists of current pulses that are aligned with the rising and falling edges of the digital pre-synaptic voltage. Then, we consider the case where $b^{2\pi}(\theta)$ consists of a train of Dirac pulses:

$$b^{2\pi}(\theta) = \sum_{n=0}^{\infty} p(\theta - n2\pi) \quad (31)$$

With:

$$p(\theta) = Q(\delta(\theta) - \delta(\theta - \pi)) \quad (32)$$

Under this assumption, (30) becomes:

$$\frac{d}{dt}\Delta\phi = \frac{Q}{T} \left(v^{2\pi}(\Delta\phi) - v^{2\pi}(\Delta\phi + \pi) \right) \quad (33)$$

In SKONN, the analog input oscillation is a symmetric triangular waveform that has a simple 2π -periodic PPV expressed as follows:

$$v^{2\pi}(\theta) = \beta_0 \text{square}(\theta) \quad (34)$$

Where:

$$\text{square}(\theta) = \begin{cases} -1, & \text{if } 0 < \theta < \pi \\ +1, & \text{if } \pi < \theta < 2\pi \end{cases} \quad (35)$$

And β_0 is the phase shift induced by the injection of 1 coulomb to the oscillating node. Finally, we express the phase dynamics of the driven oscillator:

$$\frac{d}{dt} \Delta\phi = 2\beta_0 \frac{Q}{T} \text{square}(\Delta\phi) \quad (36)$$

We notice that the average of the phase dynamics are very similar to the Kuramoto model except that its sinusoidal interaction term is replaced by a *saturated* square function in our case.

Proposition 1. *If the injected charge $Q \neq 0$ then the two SKONN oscillators admit a unique stable fixed-point $\Delta\phi^* = (\phi_i - \phi_j)^*$ such that:*

$$\Delta\phi^* = \begin{cases} 0, & \text{if } Q > 0 \\ \pi, & \text{if } Q < 0 \end{cases} \quad (37)$$

Proof. The proof consists in finding a Lyapunov function for the dynamics (36). Consider the bounded continuous Lyapunov function:

$$E = 2\beta_0 \frac{Q}{T} \text{triangle}(\Delta\phi) \quad (38)$$

With:

$$\text{triangle}(\theta) = \begin{cases} \theta - \pi/2, & \text{if } 0 \leq \theta \leq \pi \\ 3\pi/2 - \theta, & \text{if } \pi \leq \theta \leq 2\pi \end{cases} \quad (39)$$

We have :

$$\frac{\partial E}{\partial \Delta\phi} = -2\beta_0 \frac{Q}{T} \text{square}(\Delta\phi) = -\frac{d\Delta\phi}{dt} \quad (40)$$

E is minimized through time as follows:

$$\frac{dE}{dt} = \frac{\partial E}{\partial \Delta\phi} \frac{d\Delta\phi}{dt} = -\left(\frac{d\Delta\phi}{dt}\right)^2 \leq 0 \quad (41)$$

1. If $Q > 0$, the minima of E are $\Delta\phi^* = 0 [2\pi]$ and correspond to the phase fixed points of the dynamics (36).
2. If $Q < 0$, the minima of E are $\Delta\phi^* = \pi [2\pi]$ and correspond to the phase fixed points of the dynamics (36).

□

In other words, propagating a spike train that consists of positive and negative current spikes spaced in time by $T/2$ induce an in-phase or out-of-phase locking, depending on the polarity of Q . The latter can be set by choosing one of the two complementary digital post synaptic voltages as shown in Fig 3.

C.2 N coupled oscillators

When an oscillator i is perturbed by N other oscillators with same pulsation ω_0 , (28) can be generalized in the scalar case:

$$\frac{d}{dt} \alpha_i = \sum_{j=1}^N v_{ij}^{2\pi}(\phi_i) b_j^{2\pi}(\phi_j) \quad (42)$$

Similarly to the two-oscillators case, averaging out the previous equation along the fast variable ϕ_j leads to:

$$\frac{d}{dt} \alpha_i = \sum_{j=1}^N \frac{1}{2\pi} \int_{-\pi}^{\pi} v_{ij}^{2\pi}(\Delta\phi_{ij} + \phi_j) b_j^{2\pi}(\phi_j) d\phi_j \quad (43)$$

We use the spike train expression (31) to obtain:

$$\frac{d}{dt} \alpha_i = \frac{1}{2\pi} \sum_{j=1}^N \left(v_{ij}^{2\pi}(\Delta\phi_{ij}) - v_{ij}^{2\pi}(\Delta\phi_{ij} + \pi) \right) \quad (44)$$

As we inject pre-synaptic signals to the same node, we have $v_{ij}^{2\pi} = v^{2\pi}$ and we use the SKONN oscillator PPV $v^{2\pi}$ (34) to finally get:

$$\frac{d}{dt} \phi_i = \frac{2\beta_0}{T} \sum_{j=1}^N Q_{ij} \text{square}(\phi_i - \phi_j) \quad (45)$$

Note that we omitted the term ω_0 in the right-hand side of (45) as in practice we refer to the relative phase relationship between oscillators instead of the absolute values that linearly increase with $\omega_0 t$.

Considering SKONN's hardware implementation, we saw that β_0 is equal to:

$$\beta_0 = \frac{\pi}{\Delta V C_L} \quad (46)$$

And:

$$Q_{ij} = V_{DD} C_{ij} \quad (47)$$

Where ΔV is the peak-to-peak triangular amplitude at the input, C_L is the neuron input capacitance, V_{DD} is the digital voltage swing, and C_{ij} is the synaptic capacitance value. SKONN's phase dynamics become:

$$\frac{d}{dt} \phi_i = \omega_0 \frac{V_{DD}}{\Delta V} \sum_{j=1}^N \frac{C_{ij}}{C_L} \text{square}(\phi_i - \phi_j) \quad (48)$$

SKONN has an interesting phase binarization property resumed in the following proposition:

Proposition 2. Consider a neuron i of degree D , i.e. driven by D neurons j with weighted charges $Q_{ij} \in \{-q, +q\}$ $q \neq 0$.

1. If D is odd and $d\phi_i/dt = 0$, then there is at least one input neuron j such that $(\phi_i - \phi_j)$ is a multiple of π .
2. If D is even, then there is at least one ϕ_i and one set of input phase ϕ_j such that $d\phi_i/dt = 0$ and $\forall j (\phi_i - \phi_j)$ is not a multiple of π .

Proof. 1. By assuming the opposite, i.e. that $\forall j (\phi_i - \phi_j) \neq 0 [\pi]$, it leads to $\forall j \text{square}(\phi_i - \phi_j) = \pm 1$, using (4). Noticing that $D = m + l$ with $m \neq l$, and writing SKONN's phase dynamics (7) leads to:

$$\frac{d\phi_i}{dt} = 0 \implies \sum_{j=1}^D \pm 1 = \sum_{j=1}^m 1 - \sum_{j=1}^l 1 = 0 \quad (49)$$

Which is not possible as $m \neq l$ and proves the proposition.

2. Consider the integers m and l such that there are m weights $Q_{ij} = +q$ and l weights $Q_{ij} = -q$, with $D = m + l = 2k$. We can choose:

- (a) $\phi_j = 0$ for the l (resp. m) input neurons.
- (b) $\phi_j = \pi$ for $k - l$ (resp. $k - m$) other input neurons.
- (c) $\phi_j = 0$ for the remaining k input neurons.

From SKONN's phase dynamics (7) we obtain:

$$\begin{aligned} \frac{T}{2\beta_0} \frac{d\phi_i}{dt} &= -q \sum_{j \leq l} \text{square}(\phi_i) \\ &\quad + q \sum_{l < j \leq k} \text{square}(\phi_i - \pi) \\ &\quad + q \sum_{k < j \leq 2k} \text{square}(\phi_i) \end{aligned}$$

Assuming that $\phi_i \neq 0 [\pi]$, it follows from (4):

$$\begin{aligned} \frac{T}{2\beta_0} \frac{d\phi_i}{dt} &= -ql(\pm 1) - q(k-l)(\pm 1) + kq(\pm 1) \\ &= 0 \end{aligned}$$

□

D Sub Harmonic Injection Locking in SKONN

To binarize the phases, one can inject a signal at twice the oscillating frequency $V_{SHIL}(t) = A \sin(4\pi\omega_0 t)$ to an oscillator's node for which its scalar PPV contains a second-order harmonic $P_2 \neq 0$ in its Fourier decomposition [31]. In SKONN, we cannot inject the 2-SHIL signal to the input oscillating node $V_i^{in}(t)$ as the associated scalar PPV only contains odd harmonics (square (25)). In practice, we inject the 2-SHIL signal to a biasing node that allows SKONN binary phase locking. In this case, the SKONN Lyapunov function becomes

$$E = \frac{\beta_0}{T} \sum_{i,j}^N Q_{ij} \text{triangle}(\phi_i - \phi_j) + \sum_i^N A_i P_2 \cos(2\phi_i) \quad (50)$$

When SHIL amplitudes A_i are large enough, phases are binarized $\phi_i = (1 - S_i)\pi/2 \in \{0, \pi\}$ and the SKONN Lyapunov function corresponds to the Ising Hamiltonian H with an additional offset:

$$E = -\frac{\pi\beta_0}{2T} \sum_{i,j}^N Q_{ij} S_i S_j + \sum_i^N A_i P_2 = H + \text{constant} \quad (51)$$

E Impact of SKONN's limited bandwidth

When SKONN is implemented in hardware, we observe some phase deviation with respect to the theoretical phase fixed points, as shown in Fig.14. The main reason is the hysteresis block that does not switch instantaneously when the synaptic current spikes induce voltage jumps above or below the hysteresis thresholds V_H and V_L . To better understand this phenomenon, we ran two transistor-level simulations of two coupled neurons in feed-forward mode with a strong weight $W_{21}=+15$ and different frequencies (Fig.14). When the oscillation frequency is low (300 kHz), the hysteresis switching delay is negligible and there is only a small phase deviation $\delta\phi=4^\circ$. However, when the oscillation frequency increases to 1.2 MHz, the limited bandwidth of the hysteresis circuit causes a switching delay and a larger phase deviation $\delta\phi=13^\circ$.

For a given phase precision required by the application, this error could be mitigated by increasing the bandwidth of the hysteresis circuit or slowing down the oscillators, and constitute a trade-off with the energy consumption [16]. Interestingly, we have observed in experiments that having recurrent synapses $W_{ij} = W_{ji}$ compensate the hysteresis delay induced in both neurons and the theoretical phase fixed point is reached in that case (see Fig.6c and d).

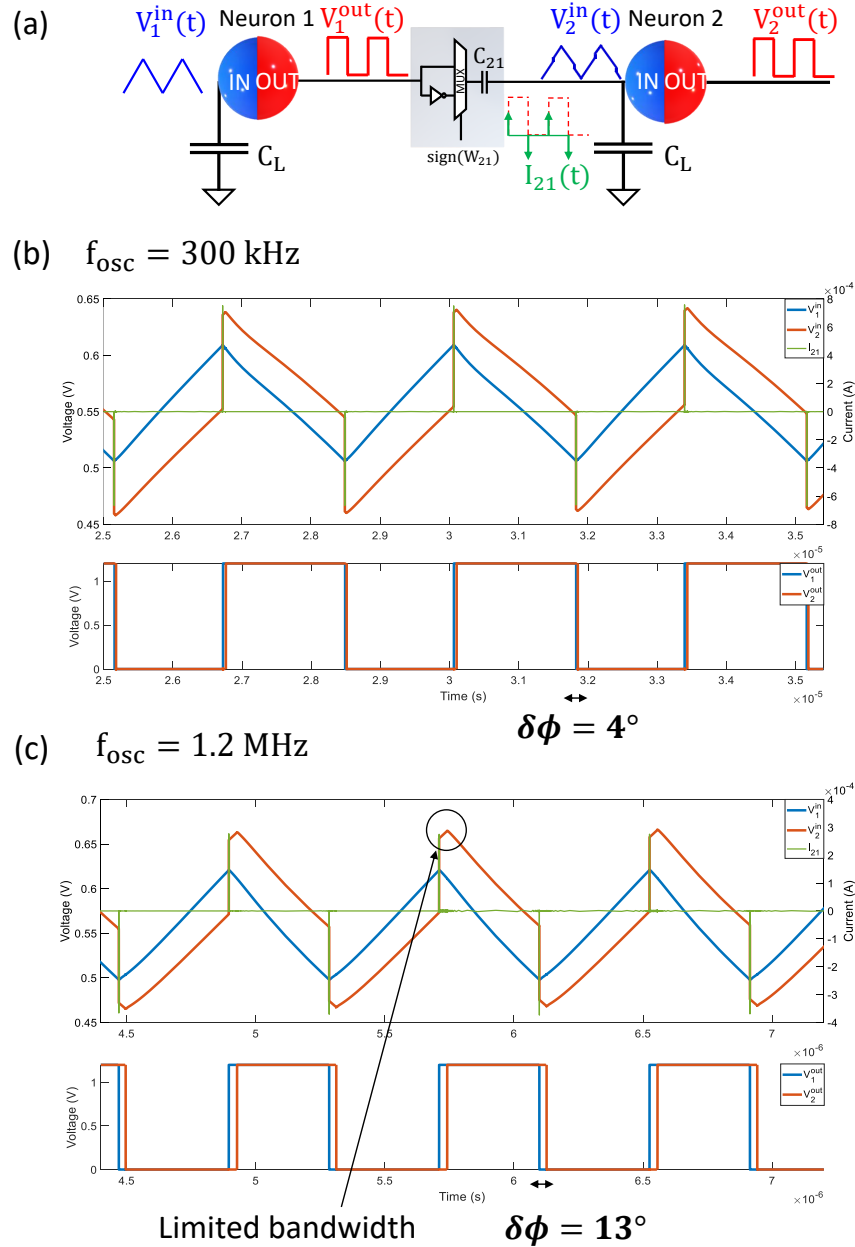


Figure 14: a) Two coupled oscillator in feed-forward mode with $+C_{21}=7.5\%C_L$ which implements $W_{21}=+15$ in the ASIC. b) Transistor-level simulation with $C_L=2\text{pF}$ to decrease the frequency to $f_{osc}=300 \text{ kHz}$. c) Transistor level simulation in nominal case where $C_L=500\text{fF}$ and $f_{osc}=1.2 \text{ MHz}$.